communications materials

Review article

https://doi.org/10.1038/s43246-024-00459-7

Advances in 3D silicon-based lithium-ion microbatteries

Check for updates

Andam Deatama Refino [1,2] ✉, Calvin Eldona [3], Rahmandhika Firdauzha Hary Hernandha [4], Egy Adhitama [5,6], Afriyanti Sumboja[7,8], Erwin Peiner [1] & Hutomo Suryo Wasisto [9] ✉

Miniaturization of modern microelectronics to accommodate the development of portable and smart devices requires independent energy storage that is compact, lightweight, reliable, and integrable on-chip. Three-dimensional lithium-ion microbatteries are considered as promising candidates to fill the role, owing to their high energy and power density. Combined with silicon as a high-capacity anode material, the performance of the microbatteries can be further enhanced. In this review, the latest developments in three-dimensional silicon-based lithium-ion microbatteries are discussed in terms of material compatibility, cell designs, fabrication methods, and performance in various applications. We highlight the relation between device architecture and performance as well as comparison between different fabrication technologies. Finally, we suggest possible future studies based on the current development status to provide a research direction towards further improved three-dimensional silicon-based lithium-ion microbatteries.

In the midst of fast evolution of artificical intelligence (AI) and internet of things (IoT), micro-/nanoelectromechanical systems (MEMS/NEMS) including electronics and sensors play a crucial role in portable and wearable devices[1–8]. The miniaturization of such devices can only be possible by realizing independent energy-storage systems that are not only fulfilling the energy requirement but are also small and could be integrated on-chip[9–12]. Current developments of energy storage devices are mainly concentrated to tackle the problems of lithium-ion batteries (LIBs) for high power purposes in kilowatt regimes such as renewable energy or electric vehicles[13–15]. Meanwhile, the so-called micro-lithium-ion-battery (micro-LIB) emerges as a more promising candidate to energize smart devices since it can provide power in micro- to milliwatt regimes with a relatively small footprint area[16]. The fabrication of such a small energy storage device is not as simple as reducing the size of a conventional battery[17]. Different challenges exist from the performance and fabrication point of view, which require optimization. Furthermore, the ability of micro-LIBs to be fully integrated into electronic circuits, where other components such as sensors and transducers are packed into a small footprint area, needs to consider many aspects for example the areal capacity, efficiency, and heat distribution[18,19]. The addition of an electrochemical cell into a dry electrical environment also needs to consider the safety aspect. Durability is of paramount importance since on-chip integration disables the easy replacement possibility of micro-LIB components. Hence, the lifetime of the battery is highly concerned. From the processing point of view, the compatibility of micro-LIB fabrication needs to comply with the existing semiconductor fabrication technology. The ability to upscale micro-LIB fabrication can highly influence production cost, which can also affect the interest of the market. Here, high-throughput production of micro-LIBs is preferable.

The early development of micro-LIBs can be traced back to the first thin-film battery produced by Liang and Bro in 1969[20]. They produced Li/LiI/AgI cells and introduced the concept of the solid-state thin-film battery. Since then, the development of sandwiched structures has become more popular and continued until the 2000s. The early modified structure in the form of an in-plane interdigitated architecture was proposed by Nakano

[1]Institute of Semiconductor Technology (IHT) and Laboratory for Emerging Nanometrology (LENA), Technische Universität Braunschweig, Hans-Sommer-Straße 66, 38106 Braunschweig, Germany. [2]Engineering Physics Program, Institut Teknologi Sumatera (ITERA), Jl. Terusan Ryacudu, Way Huwi, Lampung Selatan, 35365 Lampung, Indonesia. [3]School of Materials Science and Engineering, Nanyang Technological University, 50 Nanyang Avenue, 639798 Singapore, Singapore. [4]Department of Materials Science and Engineering, National Yang-Ming Chiao Tung University, 1001 University Road, Hsinchu 30010, Taiwan. [5]University of Münster, MEET Battery Research Center, Institute of Physical Chemistry, Corrensstr. 46, 48149 Münster, Germany. [6]University of Münster, International Graduate School for Battery Chemistry, Characterization, Analysis, Recycling and Application (BACCARA), Corrensstr. 40, 48149 Münster, Germany. [7]Material Science and Engineering Research Group, Faculty of Mechanical and Aerospace Engineering, Institut Teknologi Bandung, Jl. Ganesha 10, 40132 Bandung, Indonesia. [8]Research Collaboration Center for Advanced Energy Materials, Institut Teknologi Bandung, Jl. Ganesha 10, 40132 Bandung, Indonesia. [9]PT Nanosense Instrument Indonesia, Umbulharjo, 55167 Yogyakarta, Indonesia. ✉e-mail: andam.refino@tu-braunschweig.de; h.wasisto@nanosense-id.com

et al. in ref. 21. The idea was to increase energy and power density by employing different materials and processing techniques to produce a three-dimensional (3D) structure[22–26]. With regard to the anode, many researchers have explored materials such as TiO_2 nanotubes due to their favorable operational potential, cost-effectiveness, and non-toxic properties[27]. However, their notable drawbacks (i.e., poor conductivities) hinder their further application as they impede charge transfer. Conversion-reaction anodes, such as transition-metal oxides and sulfides, can also store high concentrations of ions. However, their practical use in microbatteries is hindered by significant, typically 30% to 50%, irreversible capacity loss during the initial cycles[28]. Metallic zinc (Zn) and aluminum (Al) can also be potential candidates as they exhibit remarkable stability in atmospheric conditions due to the formation of protective oxide layers on their surfaces. This stability is a significant advantage for the large-scale production and processing of Zn and Al metal anodes, essential for achieving higher energy densities. However, the challenge of poor reversibility is a common issue in Zn anodes and various other metal batteries. Apart from previously mentioned anode materials, alloying-type anodes like Si, Sb, Ge, and Sn can also be considered as they provide high capacity and stability[29]. Si has become one of the most promising candidates for micro-LIB applications because of its high material maturity and compatible processing tools in the semiconductor industry, which enable standard wafer-scale production. Besides, Si-based anodes have a higher theoretical capacity than the conventional graphite-based anodes. It has been demonstrated that the theoretical capacity of the Si anode is 3590 mAh g^{-1} ($Li_{3.75}Si$) at room temperature, which is almost ten times higher than that of the carbon-based anode (376 mAh g^{-1}, LiC_6)[30]. Moreover, Si has a relatively low lithiation potential (<0.5 V) vs. Li/Li^+, which makes it promising to provide a high energy density. Si is the second most abundant element in earth's crust only below oxygen, and environmentally friendly. Despite having all those advantages, Si anodes often suffer from the extreme volume expansion during lithiation of up to 300% that is also a direct consequence of its high capacity in storing Li[31]. In most cases, this volume change introduces stresses, initiates cracks, and compromises its mechanical integration[32]. Consequently, disconnection from the current collector and build-up of a thick passivating layer can occur resulting in battery performance degradation over multiple charge/discharge cycles. Moreover, in its pristine form, Si has a relatively low conductivity, which is not preferable in electrochemical cells. To overcome these challenges, many strategies have been attempted (e.g., the incorporation of other materials and the reduction of size to micro-/nanoscale)[33,34]. The former strategy is mainly intended to alter the electrochemical properties of Si, e.g., to increase its conductivity through doping or coating[35,36]. Meanwhile, the latter strategy is carried out to provide void spaces to buffer the volume change of Si and to increase surface area[37]. Therefore, numerous studies have been dedicated to incorporating different methods to fabricate the so-called 3D Si micro-LIB. However, the open question still remains on which micro-/nanostructures can deliver optimal performance in terms of specific capacity, cycling stability, and processing complexity.

In this review, the discussion is focused on the recent progress of 3D Si-based high-capacity micro-LIB development. In the first section, a quick look at the basic principle of the LIB, the device architecture, and an overview of design rules are described to serve as a context for the following discussions. Here, the general advantages of 3D over planar structures are highlighted. Secondly, the mostly studied materials for the different components of the battery are mentioned, where the benefit and challenges of their fabrication methods are also addressed. The third part will be focused on the applications of 3D Si micro-/nanostructures for micro-LIBs where different anodes, including interdigitated, vertical and coaxial pillars, rolled, and other unique structures, are compared in terms of their fabrication methods and electrochemical performance. Finally, the key development aspects of 3D Si micro-LIB are summarized and the remaining challenges are pointed out to provide a direction for further research.

Concept and fabrication of 3D Si micro-LIB

Concept of microbattery

The working principle of the micro-LIB resembles the principle of a conventional LIB, in which lithium ions are transported between electrodes during charging and discharging processes, involving externally conducted electricity either by an applied potential or as a spontaneous current flow, respectively[38]. Hence, the basic structure of micro-LIB is a planar structure that consists of two electrodes separated by a separator and an electrolyte in between. The typical reactions that occur in a micro-LIB are written as follows:

$$\begin{aligned} \text{Cathode}: \mathrm{LiM} &\leftrightarrow \mathrm{Li_{1-x}M} + \mathrm{xLi^+} + \mathrm{xe^-} \\ \text{Anode}: \mathrm{A} + \mathrm{xLi^+} + \mathrm{xe^-} &\leftrightarrow \mathrm{Li_xA} \\ \text{Total}: \mathrm{LiM} + \mathrm{A} &\leftrightarrow \mathrm{Li_{1-x}M} + \mathrm{Li_xA} \end{aligned} \quad (1)$$

where M and A are the positive electrode (cathode) and negative electrode (anode) materials, respectively. Charging occurs when the cathode material is oxidized and releases lithium ions due to an applied voltage. The lithium ions then diffuse through the electrolyte and the electrons are driven through an external circuit, both to the anode material. The reduction reaction arises at the anode where the lithium ion is converted back to the atomic lithium, which is intercalated/alloyed with the anode material, forming Li_xA (see Eq. (1)). The discharging process occurs in the opposite direction spontaneously when both electrodes are connected, producing usable electricity. In a half-cell configuration, lithium metal is usually operated as a counter electrode. In this case, the anode material is employed as a working electrode and the lithium metal acts as an anode due to its lower potential compared to the Li_xA, and the lithium migration to the A is regarded as a discharging process.

The capability measure of an energy storage system to store electric charge is known as capacity. In battery research, commonly, the specific capacity of different materials is compared in terms of their weights (i.e., specific capacity/gravimetric capacity (C_m)), which is usually represented by the unit mAh g^{-1}. Moreover, when the volume is considered to be more important, the specific capacity can also be converted into the charge density/volumetric charge capacity (C_v) that is usually represented by the unit mAh cm^{-3} based on Eq. (2):

$$C_v = \rho \times C_m \quad (2)$$

where ρ is the active material density. However, in contrast to conventional batteries, the areal footprint is more of a concern in semiconductor technology. Hence, areal capacity (C_a) is more suitable to be used as a capacity metric in micro-LIB and can be estimated by Eq. (3):

$$C_a = t \times \rho \times C_m \quad (3)$$

where t is the active material thickness.

Furthermore, the areal energy density (E_a, Wh cm^{-2}) can be calculated as:

$$E_a = V \times C_a \quad (4)$$

with V is the potential difference between the anode and the cathode measured over time. Besides areal energy density, another important parameter in micro-LIB is the areal power density (W cm^{-2}), which represents the amount of energy that can be delivered per unit area per unit time. Therefore, it depends on the current density. Improving both of these parameters (i.e., areal energy and areal power densities) is the aim of producing a high-performance micro-LIB.

Material selection is the early step to achieving improvement in micro-LIB performance. The reason is that both voltage and specific capacity are intrinsic properties of materials. Hence, the determination of material highly influences the energy and power density of a micro-LIB. Firstly, the design of a micro-LIB needs to consider the capacity of both cathode and anode

materials. As both of them act as the container for the working ion (i.e., Li^+ ion), the capacity of a battery is determined by the capacity of either the anode or the cathode (depending on which side has the lower capacity). Higher areal capacity contributes to higher areal energy density (see Eq. (4)). Secondly, it is also important to consider the nominal voltage, i.e., the voltage difference between the cathode and the anode. The voltage (also known as the open-circuit voltage) of a micro-LIB can be estimated by taking the difference between the electrochemical potential vs. Li/Li^+ of the cathode and the anode. In a full-cell configuration, the cathode has a higher potential compared to the anode. Hence, higher cathode potential and lower anode potential result in higher potential difference contributing to larger energy density. The electrolyte material also contributes to the battery performance (i.e., the power density). Since ions move much slower in the electrolyte than electrons that are conducted through the external circuit, the current density is more determined by the ionic conductivity of the electrolyte. In general, a higher ionic conductivity of the Li^+ ions in an electrolyte can lead to higher current density of a micro-LIB, and therefore higher power density.

As a potential anode material in LIBs, Si had attracted the attention of many studies. In contrast with the intercalation of Li (i.e., Li intercalates between adjacent atomic layers) in graphite, the lithiation mechanism of Li^+ ions into Si occurs through insertion process. Lithiation mechanism of Si in general is a Li-Si alloying reaction, involving Si-Si bond breaking. Works have been done to investigate the electrochemical characteristics of crystalline Si (*c*-Si) with the aims of understanding the lithiation mechanism and improving Si anode performance in LIBs. Since the performance of a Si anode is limited by the mechanical disintegration of Si upon (de-)lithiation, studies are dedicated to demystify the lithiation-induced stresses. It was found that the strain evolution in *c*-Si is highly anisotropic[39]. This non-uniform deformation drives gradient strain fields, which determine the material performance. Si nanopillars with three different axial orientations (i.e., < 100 > , <110 > , and <111 >) were used to investigate the morphological deformation of *c*-Si upon lithiation[40]. The cross-sectional view of Si nanopillars after the first lithiation shows cross, oval, and hexagonal shapes of <100 > , <110 > , and <111> oriented nanopillars, respectively. The results suggest an orientation-dependent nature of lithiation, in which Li prefers to enter into *c*-Si through <110> ion channels. Furthermore, atomistic insight into the (de-)lithiation mechanism of Si nanowires was obtained by reactive molecular dynamic simulation[41] that confirms a Li penetration tendency along the <110> and <112> directions. During lithiation, *c*-Si transforms into amorphous Li_xSi (*a*-Li_xSi) phases through Si-Si bond breaking caused by tensile stress between Si atoms. In situ transmission electron microscopy (TEM) was used to observe the dynamics of lithiation at atomic resolution in real time[42]. The study revealed the so-called ledge mechanism, in which an amorphization of *c*-Si during Li insertion occurs via a layer-by-layer peeling of {111} atomic planes at the *c*-Si/*a*-Li_xSi interface. It was also demonstrated that the progression of the reaction front is atomically sharp (~1 nm), and its mobility depends on crystal orientation (i.e., amorphizations through {111} facets are much slower than the {110} and {112} facets). Besides *c*-Si, amorphous Si (*a*-Si) is also used as an anode in LIBs[43]. Similar to *c*-Si, the first lithiation of *a*-Si is also characterized by a two-phase reaction with the progression of a sharp interface into the non-lithiated Si, followed by a single-phase mechanism in the delithiation process and the subsequent cycles. However, there are some differences including isotropic lithiation and volume change, lower Li concentration in the lithiated phase compared to the lithiated *c*-Si, and a relatively constant reaction rate (in contrast to the significant slowing of the reaction front in *c*-Si). The benefit of those characteristics is that *a*-Si has a more manageable morphological deformation than *c*-Si, which in some cases, makes *a*-Si more favorable as an anode material. For example, it was demonstrated that Si nanoparticles in an amorphous phase have a larger critical radius for fracture compared to their crystalline counterparts.

To maximize energy density, cathodes for LIBs are engineered to have higher average potentials relative to Li/Li^+ compared to earlier materials like TiS_2 and vanadates designed for lithium metal batteries[44]. Moreover, cathode materials are typically limited to those containing first-row transition metals, including manganese (Mn), iron (Fe), cobalt (Co), and nickel (Ni), to meet the demand for high specific capacity[45]. Presently, cathode materials for LIBs encompass metal oxides and poly-anionic compounds. Integrating cathodes into microbattery assemblies represents a notable challenge in microbattery development. Thus far, only a handful of instances have been documented regarding the use of 3D cathode architectures for microbatteries, as achieving a 3D cathode poses a severer difficulty than synthesizing 3D anodes or electrolytes. This section provides an overview of potential cathode materials that can be paired with silicon-based anodes in 3D Si micro-LIBs (refer to Table 1). The suitability is assessed based on various parameters such as average potential, average specific capacity, gravimetric energy density, cost-effectiveness, safety consideration, and material synthesis. The gravimetric energy densities are obtained from the references, where those values were calculated as the product of average potential and specific capacity[46]. Figure 1 offers a qualitative comparison of these cathode materials.

A promising alternative approach involves the creation of 3D LIBs with thicker electrodes, surpassing 100 μm in thickness[47–51]. The volumetric ratio of active to inactive materials within LIBs, and consequently their energy capacity, increases linearly with the electrode thickness for a given area. However, achieving efficient ionic and electronic transport through thicker electrodes presents challenges, leading to limitations in power density[52–54]. To address this, recent research has concentrated on producing lithium-based cathodes with internal open channels perpendicular to current collector surfaces. This was accomplished through magnetic-field-induced alignment of anisotropic porogens, comprising either magnetic particle-coated polymer rods or particle-stabilized emulsion droplets. The result was sintered $LiCoO_2$ (LCO) cathodes, measuring 310 μm in thickness, exhibiting an impressive areal capacity of ≈12 mAh cm^{-2} at a rate of 0.1 C[55]. In the pursuit of enhancing electronic transport, highly porous metal foams have also been employed as 3D current collectors to develop high-performance $LiFePO_4$ (LFP) cathodes, 540-μm-thick, with an areal capacity of 8.8 mAh cm^{-2} at a current density of 1 mA cm^{-2}[47]. It is worth noting that the use of thick electrodes introduces additional challenges, including issues with migration, cracking, and delamination during the drying process[56], as

Table 1 | Commercial lithium-ion battery cathode materials in different structures[44–46,83,169–172]

Cathode material	Structure	Average potential vs Li/Li^+ (V)	Specific capacity range (mAh g^{-1})	Gravimetric energy density range (Wh kg^{-1})	Cost	Safety	Material synthesis
LCO	Layered	3.90	140–160	530–550	High	Low	Easy
LFP	Olivine	3.45	150–170	520–590	Low	High	Medium
NCA	Layered	3.80	180–200	680–760	Medium	Medium	Medium
LMO variants	Spinel	4.10	100–120	410–490	Low	Medium	Easy
NCM variants	Layered	3.80	160–170	610–650	Medium	Medium	Medium
$LiNiO_2$	Rocksalt	3.85	150–190	620–770	Medium	Low	Difficult

A comparison of several key performance indicators (i.e., average potential vs. Li/Li^+, specific capacity range, and gravimetric energy density) of different cathode materials (i.e., $LiCoO_2$ (LCO), $LiFePO_4$ (LFP), $Li(Ni_{0.80}Co_{0.15}Al_{0.05})O_2$ (NCA), $LiMn_2O_4$ (LMO) variants, $LiNi_{1/3}Co_{1/3}Mn_{1/3}O_2$ (NCM) variants, and $LiNiO_2$).

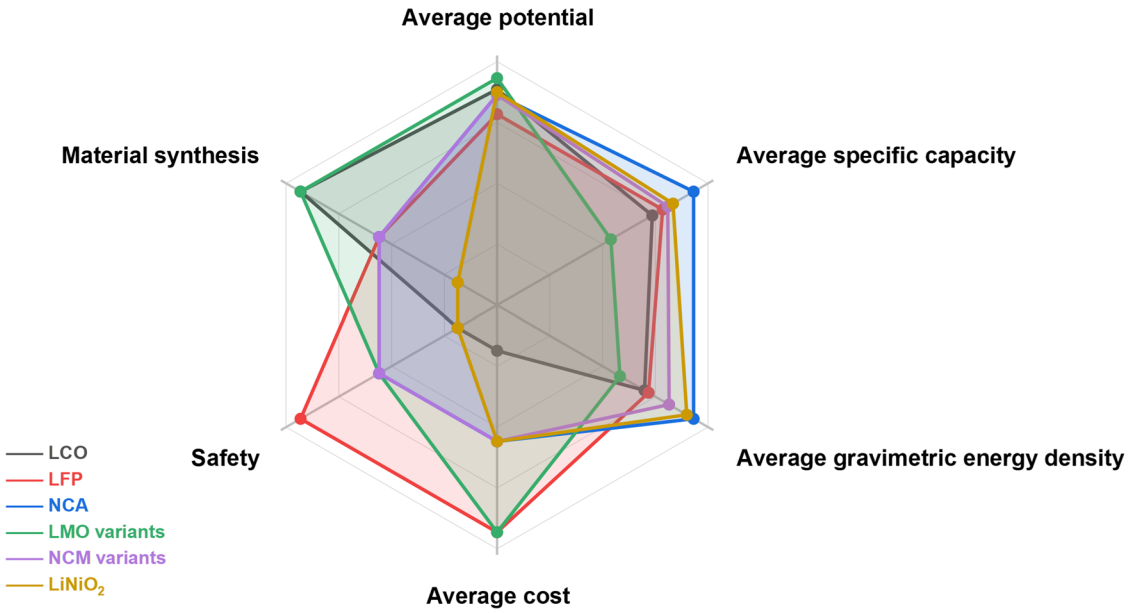

Fig. 1 | Cathode-material performance comparison for supporting 3D Si micro-LIBs. Different cathode materials have their own advantages and drawbacks in terms of lifespan, energy density, performance, cost, and safety.

well as incomplete electrolyte infiltration[57]. Another strategy for achieving uniform deposition of LCO involves the thermal decomposition of sol-gel precursors spray-coated onto 3D-Al-nanorod current collectors directly grown on Al substrates. Additionally, it is important to recall that Ceder et al. have identified new cathode materials, in which non-transition metals are substituted for cobalt[58]. Phases such as $LiCo_{1-x}Al_xO_2$ have been reported, and an increase in cell voltage with Al substitution has been experimentally confirmed. Compared with a planar electrode presenting an equivalent nominal capacity, a 3D electrode exhibits improved capacity retention, retaining 68% of the nominal capacity at 8 C instead of 11%[59].

Recent studies have showcased the creation of micro-LIBs through the direct deposition of LFP cathode and $Li_4Ti_5O_{12}$ (LTO) anode inks. The cathode inks are formulated by suspending LFP nanoparticles (with an average diameter of 180 nm) in a solution containing deionized water, ethylene glycol, glycerol, and viscosifiers derived from cellulose. This process involves multiple steps, including particle dispersion, centrifugation, and homogenization. Specifically, high-aspect-ratio, interdigitated LFP and LTO electrodes were printed with a wall thickness of approximately 60 µm and a height ranging from around 200 to 400 µm. These micro-LIBs, with a total volume of less than 1 mm^3, demonstrated an areal capacity of roughly 1.5 mAh cm^{-2} when discharged at rates below 5 C. However, electronic transport constraints were observed, as LFP electrodes printed with eight layers (approximately 200 µm thick) displayed the same current density as those with 16 layers (approximately 400 µm thick)[60]. Besides its promising performance, several challenges for LFP, such as low electronic conductivity and limited Li-ion diffusivity, especially for untreated/undoped LFP, which affect the overall properties of LFP, have to be addressed for future applications[61–64].

In another investigation, $Li(Ni_{0.80}Co_{0.15}Al_{0.05})O_2$ (NCA) was employed as an active material for the positive electrode in a semiconductor-grade single-crystalline Si microbattery. The NCA cathode was created using a conventional slurry formulation, comprising 88% w/w NCA, 6% polyvinylidene fluoride (PVDF), 3% carbon black, and 3% graphite, mixed with an equal weight of N-methyl-2-pyrrolidone (NMP). The slurry mixture was prepared using a planetary micro mill. The quantity of NCA within the cathode cavity was either 3.8 mg (for cells with a 0.5 mAh capacity) or 10.0 mg (for cells with a discharge capacity ranging from 1.0 to 2.0 mAh). The slurry was then dried at 60 °C for 12 h in a temperature chamber without forced air circulation. The device exhibited a high current output power (200 mW cm^{-2}; 30 mA peak current) and demonstrated robust charge/discharge stability for at least 100 cycles (equivalent to 10 mAh cm^{-2}). Additionally, it exhibited a high Coulombic efficiency, nearing 100%, making it highly suitable for integration into a wide array of intelligent, self-powered electric devices[65]. Using a similar approach, the cathode slurry consisted of 75% NCA, 18.3% graphite, 1.7% PVDF, 2.8% lithium bis(trifluoromethane)sulfonimide (LiTFSI), 1.1% tetraglyme (TG), and 1.1% poly(ethylene oxide) (PEO), which were combined and assembled using a vacuum-infiltration protocol onto SU-8-coated Si arrays. The resulting rechargeable 3D microbatteries, fashioned on a 3 mm × 3 mm footprint, exhibited an areal capacity of nearly 2 mAh cm^{-2}. They operated at current densities of up to 0.66 mA cm^{-2} and maintained stability through 100 cycles[66].

An innovative 3D micro-LIB has been introduced, featuring sub-10 nm $LiMn_2O_4$ (LMO)/LTO nanocrystals synthesized through a solvothermal method and a novel copolymer gel electrolyte. This microbattery exhibited exceptional capacity retention (40% at 300 C) and possessed a high power density of 855.5 µW cm^{-2} $µm^{-1}$. The tailored microelectrodes were created via solvent-assisted imprint lithography, utilizing well-dispersed nanoparticle ink, and the battery cell was vertically integrated through layer-by-layer (LBL) assembly[67]. In a separate investigation, functional 3D LMO thin-film electrodes were produced, yielding a footprint capacity of 0.5 mAh cm^{-2}, employing an innovative process grounded in a solid-state reaction between electrolytic manganese dioxide (EMD) and Li_2CO_3 stacked-layers. These prepared thin films demonstrated outstanding electrochemical activity, achieving a volumetric capacity of 1200 Ah L^{-1}, closely approaching the theoretical capacity of spinel LMO. Moreover, a thin-film morphology, spanning a few hundred nanometers, allows for utilization of both 3 V and 4 V regions[68]. Furthermore, a Mn-dissolution process of the LMO cathode at elevated temperatures[69] has to be a concern to achieve a more applicable 3D Si micro-LIBs.

A lithium nickel manganese cobalt oxide, specifically $LiNi_{1/3}Co_{1/3}Mn_{1/3}O_2$ (NCM-111), has emerged as a pivotal cathode material, particularly for mobile power sources, owing to its notable gravimetric and volumetric capacity. However, the automotive industry necessitates batteries with even higher energy density to propel the development of electric vehicles with competitive or surpassing ranges compared to internal combustion engine automobiles[70]. NCM-111 boasts several advantages, including a cell-level high energy density (>150 Wh kg^{-1}), a robust power density (650 W kg^{-1} @ 25 °C and 50% Depth of Discharge/DoD)[71], an exceptional rate

capability, a substantial specific capacity (163 mAh g^{-1}), and a commendable thermal stability in the fully charged state[72]. One strategy to enlarge energy density is by augmenting the nickel content in the NCM cathode material. Hence, $LiNi_{0.6}Mn_{0.2}Co_{0.2}O_2$ (NCM-622) cathodes were fabricated using tape casting, incorporating 80 wt% of active material with a film thickness of 54 µm. Additionally, to attain a 3D architecture, an ultrafast fiber-laser-driven ablation process was employed, creating line structures with a pitch of 200 µm. This cathode material demonstrated an initial discharge capacity of 178 mAh g^{-1} at a C-rate of C/10. Notably, at a discharge rate of 10 C, the cell equipped with the structured cathode managed to maintain a discharge capacity of 35% of the initial value[73].

Moreover, well-established synthesis procedures[70,74–80] and stability make cathode powder materials suitable for use in various electrode production methods. There is no distinct variation in the approach to achieving a 3D architecture, even with cathodes containing higher nickel contents such as $LiNi_{0.8}Mn_{0.1}Co_{0.1}O_2$ (NCM-811), $LiNi_{0.9}Mn_{0.05}Co_{0.05}O_2$ (NCM-955), and other potential cathode materials like $LiNiO_2$[81,82]. Various protocols, including conventional slurry-based techniques, tape casting, laser ablation, layer deposition synthesis (e.g., atomic layer deposition (ALD) and molecular layer deposition (MLD)), as well as other thin-film fabrication and micro-architectural building methods, could be employed to design an advanced 3D cathode that complements the 3D Si micro-LIB[83–86].

Electrolytes are essential in batteries for transporting ions and conducting current between the positive and negative electrodes. Electrolytes can be classified into liquid and solid electrolytes. LIBs that utilize organic liquid electrolytes made of lithium salts, organic solvents, and additives, provide them with high ionic conductivity and good electrode wettability[16]. With regard to the micro-LIBs, the electrolyte lithium salts that are preferably used are lithium hexafluorophosphate ($LiPF_6$) and lithium perchlorate ($LiClO_4$)[87–89]. Both of them have several advantages compared to other electrolytes, including better stability, higher conductivity and solubility, simpler purification, and inexpensive[90]. The advantage of $LiClO_4$ over $LiPF_6$ is the absence of hydrofluoric acid (HF) or HF-related electrolyte components. This distinction is critical because HF can be corrosive and damaging to various components[91]. $LiClO_4$ enables the application of Na-, K-containing glass cell components (borosilicate glass 3.3) that are available in semiconductor manufacturing processes. This compatibility offers a unique edge in integrating battery technology with semiconductor manufacturing[65]. In 2008, Barbara Laik and her research group used a $LiClO_4$ electrolyte for micro-LIBs with Si nanowire anodes, where propylene carbonate was applied to dissolve the $LiClO_4$ electrolyte[87]. However, the strongly oxidizing properties of $LiClO_4$ limit its long-term application due to potential safety hazards, while $LiPF_6$ suffers from low thermal decomposition temperatures. In addition, liquid leakage and encapsulation complexities hinder liquid electrolytes from further utilization in micro-LIBs[90]. Solid electrolytes have proven superior to organic liquid electrolytes in various ways, making them an important component for the practical application of micro-LIBs. These advantages include their non-flammable, high-temperature stability, and non-volatile nature, eliminating the risk of combustion or explosion[92]. They also have a wide electrochemical window, which makes them more compatible with high-potential cathodes and greatly improves energy density[93]. In addition, they have enhanced mechanical rigidity, which helps to prevent dendrite growth from cycled metallic anodes[94]. Lastly, their elastic modulus is tunable, making them easier to be processed and more flexible[95]. Therefore, the exploitation of solid electrolytes is considered a promising alternative to diminishing the intrinsic safety disadvantages of liquid electrolytes while maintaining the electrochemical performances of the micro-LIBs.

Solid electrolytes are generally classified into three types, i.e., organic, inorganic, and composite solid electrolytes. Organic solid electrolytes are basically polymer-based electrolytes with various advantages (e.g., excellent ionic conductivity, good ability in maintaining volume change, flexibility, and facile fabrication)[96]. A study by Chaudoy et al. demonstrated the application of a gel polymer electrolyte (GPE) based on polyvinylidene fluoride-co-hexafluoropropylene (PVDF-HFP) linear polymer for a macroporous Si anode[97]. The findings indicate that PVDF-HFP-based GPE has a noteworthy ionic conductivity of 1.88 mS cm^{-1} at room temperature. The results demonstrate that PVDF-HFP-based GPE is well-suited to work with a negative electrode based on macroporous Si thanks to its ability to enlarge the pore size and enhance the porosity of the electrolyte membrane, resulting in a promotion of ion transport in the electrolyte[98].

In a more recent study, Hur et al. utilized solid electrolytes in the form of SU-8 polymer electrolytes[66]. An interesting SU-8 polymer that possesses a similar structure to GPE was patterned onto Si post arrays using photolithography and exhibited high conformity. When exposed to UV light, SU-8 undergoes covalent crosslinking resulting in a negative-tone photoresist behavior. SU-8 is advantageous for conformal electrolytes as it can swell with liquid electrolytes without dissolving when it is crosslinked. The bonding between neighboring SU-8 monomers is the primary factor that determines its performance. The bulk of the SU-8 monomer is robust. However, low ionic conductivity (2.8×10^{-7} S cm^{-1}) and degraded structure caused by pulverization of Si are challenges that still need to be addressed for GPE electrolytes before their further commercialization.

Inorganic solid electrolytes can be identified from their structures, which generally are crystalline and glass materials. The ionic conductivity, thermal stability, and electrochemical decomposition potential of crystalline electrolytes are typically high. Nevertheless, grain boundaries in these electrolytes can impede the transport of Li^+ ions. Therefore, to achieve relatively high overall conductivity, it is essential to establish good contact between the electrolyte and electrode[99]. On the other hand, inorganic glass electrolytes possess distinct structural benefits. Their highly defective structure creates an abundance of vacancies for Li^+ to occupy, which facilitates ion migration. These materials can exhibit continuous variation in composition, resulting in a diverse range of chemical properties. Additionally, the isotropic nature of glassy materials allows ions to diffuse uniformly in all directions, making it easier for them to pass through particle interfaces[100].

LiPON-based compounds are the most developed glass electrolytes because they have high electrochemical stability and low electronic conductivity. Phan et al. evaluated LiPONB as a solid electrolyte in Li/LiPONB/Si microbatteries[101]. Boron was added into LiPON electrolytes to improve chemical and thermal durability, while also maintaining the electrical performance[101]. The most prominent finding from this study is the ability of LiPONB to prevent initiation of cracks in the Si anode thanks to its excellent mechanical stability and adhesion. It was also found that the reaction of the LiPONB electrolyte with the electrodes does not produce any byproduct at their interfaces, implying the compatibility of LiPONB with Si anodes.

Kanazawa and coworkers recently prepared thin-film batteries consisting of amorphous vanadium oxide with lithium phosphorus oxide (VO-LiPO), Si, and LiPON as cathode, anode, and electrolyte materials, respectively[102]. The process involved the use of a three-target RF magnetron sputtering system, which had a mask moving system, to deposit multiple layers of VO-LiPO-cathode, LiPON-electrolyte, and Si-anode materials onto a substrate. It was discovered that the resulting thin-film LIBs exhibited a compact structure and well-defined boundaries between the LiPON electrolyte and both the cathode and anode layers, suggesting compatibility among them.

However, all-solid-state systems using LiPON-based electrolytes show a slightly reduced capacity for a given voltage window and a lower current density due to higher polarization caused by the lower ionic conductivity of LiPON solid electrolytes in comparison to a liquid one[101]. There are studies that have been dedicated to improve the ionic conductivity of LiPON, for example by the addition of molybdenum trioxide (MoO_3)[103] or by doping (B, Al, As, or Mg)[104,105]. Implementation of such efforts in Si micro-LIBs should be aimed in the future. Additionally, the synthesis and deposition of high-quality LiPON thin films can be technically challenging and requires specialized equipment, which can increase the cost and complexity of the manufacturing process[24]. Thus, these problems need to be resolved before their further applications for micro-LIBs.

From the perspective of mechanical stability, the employment of a solid electrolyte into Si micro-LIBs should also consider the structural integrity of the Si anode. For example, some of the state-of-the-art solid electrolytes require high stack pressures for optimal device performance that are even surpassing 100 MPa[106,107]. This might rise some questions about the viability of the Si anode to handle the pressure within the cell, especially when a 3D nano-/microstructure is utilized. It is because Si is known of its brittleness. In fact, a study showed the ability of microstructured Si of high surface quality to handle shear stress up to 4 GPa[108]. In another report, a Si nanowire with a diameter of 30 nm can even sustain an extreme tensile stress of more than 12 GPa[109]. Moreover, the feasibility of employing high stack pressures on such systems has indeed been demonstrated, which shows the capability of Si to maintain not only functional stability but also mechanical robustness upon high pressure.

In micro-LIB fabrication where semiconductor processing techniques are heavily adopted, a careful design and realization of various Si morphologies as well as material modification can be implemented in a well-defined manner. In terms of structural modification, the so-called 3D Si anode offers some benefits to the performance of micro-LIBs compared to conventional 2D designs.

Importance of 3D silicon anode

The most basic configuration of a micro-LIB is the planar laminated structure. The components are arranged simply in stacking from the bottom to the top electrodes where the electrolyte is located in between them. Both electrodes are connected to current collectors, which also act as contacts. In this sandwich structure, lithium ions move vertically through the electrolyte over the area of the micro-LIB. Improvement of areal energy density can be realized by choosing an appropriate material that will alter the areal capacity, material density, and voltage (see Eqs. (3) and (4)). The other way to realize it is by increasing the material loading. Since the areal footprint is a constraining factor for a micro-LIB, it is more sensible to an increase of thickness of the active material. However, increasing the thickness will also result in longer Li^+ ion transport pathways. Moreover, due to the dependence of the diffusion rate on the distance to the electrode-electrolyte interface, a thick electrode will hinder the reaction rate and thus lower the power density. The other challenge that occurs in thick electrodes is that the material will be more prone to structural disintegration, which can lead to film delamination, and then to capacity fading. In contrast, reducing the electrode thickness can increase the reaction kinetics as well as the power density, but at the same time lowering capacity and hence the energy density is also decreased. Finding a good balance between energy density and power density is imperative depending on the intended applications. Nevertheless, this trade-off ultimately limits the improvement of planar micro-LIB performance.

To tackle the limitation faced in the planar micro-LIB architecture, the concept of 3D electrode structure is adopted[19,110,111]. There are at least two advantages that can be obtained from such a structure. Firstly, the modification of topography by maintaining the electrode/electrolyte/electrode sandwich configuration allows a larger electrochemically active surface area within the same footprint. As a result, an increase in capacity due to a larger electrode surface can be achieved without sacrificing the Li^+ ion transport distance. This also means that one can realize higher areal energy density without giving up the areal power density (Fig. 2a). Secondly, the introduction of spaces between the electrodes in a 3D structure provides room for an expansion of the electrode, considering the fact that the alloying process of Li and Si causes an extreme volume change. This room will buffer the volume change during the charging/discharging due to the Li^+ insertion, reduce concentrated stresses, and prevent cracking of the electrode. Ultimately, the integrity of the electrode can be maintained and a capacity degradation can be suppressed. The comparison between planar and 3D structures can be evaluated by calculating their areal gain (AG). In principle, AG is the ratio between the total electrochemically active surface area (A_{active}) to the actual micro-LIB area ($A_{microbattery}$) as defined in Eq. (5).

$$AG = \frac{A_{active}}{A_{microbattery}} \tag{5}$$

The A_{active} is calculated depending on the geometry of the 3D structure, whereas the $A_{microbattery}$ is simply the footprint of the micro-LIB itself. For a

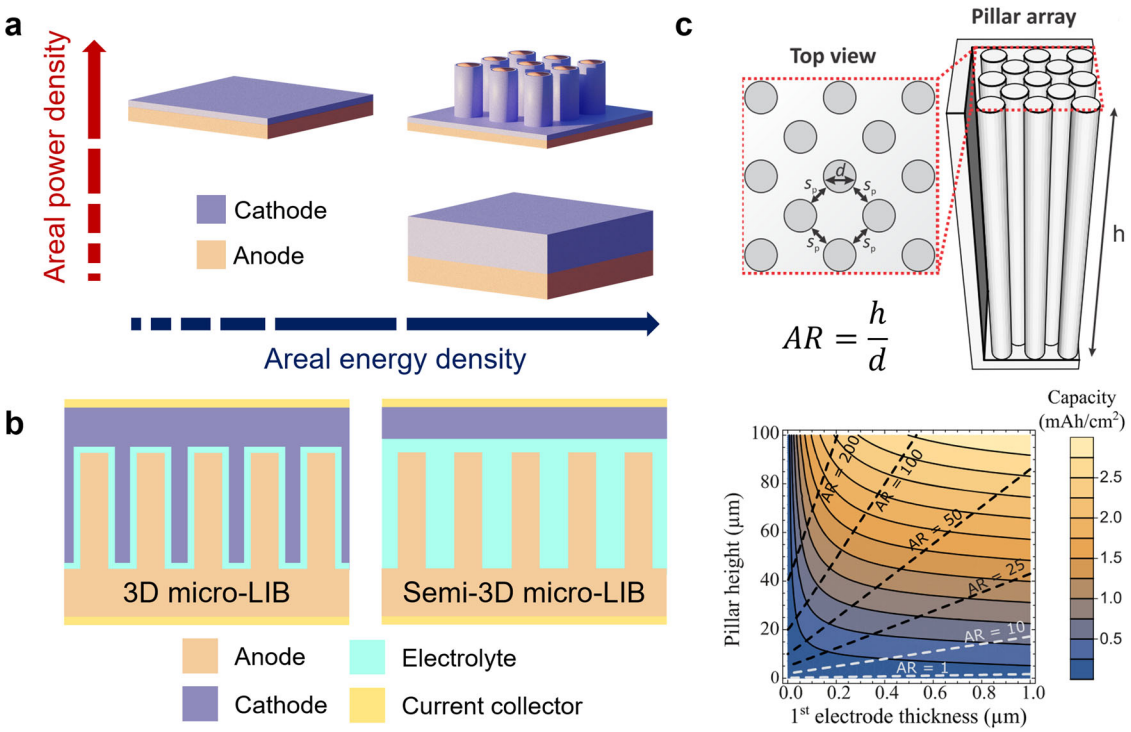

Fig. 2 | Design of 3D Si micro-LIB. a Benefit of 3D structuring to obtain both high areal power density and areal energy density. **b** Concept comparison of 3D and semi-3D Si micro-LIBs. **c** Calculation of areal capacity based on diameter and pitch of pillar arrays and the thickness of the first electrode. Adapted with permission from ref. [113]. Copyright 2019 American Chemical Society.

planar architecture, for example, AG equals to 1 because the electrochemically active area is the same as the areal footprint of the micro-LIB. When the surface is modified to a 3D structure, A_{active} will most likely increase while $A_{microbattery}$ stays the same, therefore AG will be higher than 1. Although the value of AG is not directly related to the performance of the micro-LIB, it can somehow give an idea of how different 3D architectures can yield different increases in surface area relative to the planar architecture.

Since 3D geometry influences the performance of a 3D micro-LIB, optimally designing the morphology is imperative. The basic 3D architecture is the coaxial structure, in which electrolyte and cathode thin films are conformally coated successively to a 3D anode. Yue et al. proposed an alternative called a semi-3D structure[112]. Here, instead of conformal coating, the electrolyte is completely filling the gaps between 3D structures, and the cathode is deposited on top of it as a 2D thin film. This architecture can reduce the possibility of short circuits while keeping the benefits of a large interface area of the 3D anode structures to the electrolyte (Fig. 2b). Moitzheim et al. derived a calculation based on vertical pillar architecture to investigate the effect of anode structural dimensions on micro-LIBs' capacity[113]. They modeled the vertical pillar with a coaxial structure, which means the stack of materials is conformally deposited around the pillar. They assumed that the composing components are arranged in the following order: a current collector, a cathode, a solid electrolyte, and an anode. The pillar arrays are arranged in a square lattice. Then, the capacity of the 3D micro-LIBs is given by Eq. (6):

$$C_{3D} = \frac{C_v l_1}{G}\left[1 + \frac{\pi h\left(d + l_1\right)}{\left(d + s_p\right)^2}\right] \quad (6)$$

where C_{3D} is the footprint capacity, C_v is the volumetric capacity, l_1 is the cathode thickness, G is a geometric constant ($G = 1$ for square lattice), h is the pillar height, d is the total pillar diameter, and s_p is the interpillar spacing. In this case, the smallest s_p and the optimal d are selected enabling the maximum capacity that can possibly be obtained. By assuming the $C_v = 1000$ mAh cm^{-3}, the C_{3D} is plotted as a function of h and l_1. Different aspect ratios can also be seen in Fig. 2c. In general, higher pillars and thicker cathode result in higher footprint capacity. In practice, the heights of pillars are only challenged by the fabrication method, where the electrode thickness is constrained by the spacing between pillars.

3D device fabrication

As discussed in the previous section, the design aspects (i.e., material selection and device structure) determine the performance metrics (i.e., areal energy density and areal power density) of a 3D Si micro-LIB. In addition to the performance considerations, the manufacturing of Si micro-LIB needs also to take into account the fabrication techniques, especially when mass production is of interest, as it can influence the cost-related factors (e.g., energy, time, and cost). Moreover, the fabrication of a 3D Si micro-LIB should be compatible with the semiconductor fabrication line and constrained with a small areal footprint. In semiconductor industry, the processing of Si has been very well-matured. Therefore, microstructural-modification-involving techniques such as lithography, etching, and deposition can be directly incorporated into the semiconductor production lines. Since the base material for semiconductor devices mostly come from Si wafers, the production of micro-LIBs can also be integrated directly into a micro/nanoelectronic circuit, which makes it act as an on-chip independent power source. The ease of processing on wafer scale also enables the mass production of micro-LIBs, which in turn will lower the production cost. From the fabrication point of view, Si anodes can be manufactured by various techniques depending on their desired functionalities and specific purposes in a micro-LIB. In general, the fabrication of a Si anode can be classified either as additive (bottom-up, see Fig. 3a–c) or subtractive (top-down, see Fig. 3d–f) methods. Table 2 summarizes different fabrication methods of a Si micro-LIB with their advantages and disadvantages.

Additive methods involve the deposition of Si to a substrate either physically or chemically. Physical vapor deposition (PVD) has been widely used in semiconductor industries to deposit a wide variety of materials. The characteristic of this method is the physical breaking of a solid target material (i.e., in our case, it is Si) under vacuum and its transport in the vapor phase to a substrate. Among the PVD techniques, sputtering and electron-beam (e-beam) evaporation are the most commonly used methods to fabricate the Si anode in micro-LIBs. Sputtering is a versatile method to deposit various materials on different substrates, which makes it an interesting choice for Si anode fabrication[101]. An ionized inert gas (e.g., Ar or N) is used to sputter a Si target under vacuum. In particular, radio frequency (RF) sputtering is utilized due to the limited conductivity of Si. A highly uniform and dense thin-film of *a*-Si can be deposited thanks to the high kinetic energy of the sputtered atoms, allowing a redistribution of Si atoms on the substrate. Moreover, the application of sputtering on a 3D substrate has been demonstrated. This technique, however, has its own limitations. For example in mass production, it is inefficient and costly since loss of Si during vapor phase transport is unavoidable. Also due to a low deposition rate, it takes quite a long time to deposit several hundreds of nm, which is usually required for the anode application. A larger deposition rate and a more efficient process can be achieved using evaporation methods. Instead of using ions, the breakdown of target material in the evaporation process utilizes mainly thermal energy. In thermal evaporation for example, Joule heating is used to melt the target material on a crucible. However, some materials including Si have a higher melting point than the crucible, which makes this method not applicable. Therefore, e-beam evaporation is used for Si-anode deposition by directly bombarding the target material using an electron beam[89].

Despite its similarity to PVD in terms of deposition principle, the chemical vapor deposition (CVD) uses the gaseous materials instead of solid elements as precursors. The process relies on the chemical reaction of a vapor-phase precursor at high temperature. There are several types of CVD in micro-LIB fabrication, namely metal-organic CVD, low-pressure CVD (LPCVD), laser-assisted CVD, and plasma-enhanced CVD. Baggetto et al. demonstrated the fabrication of a thin-film Si anode on a 3D substrate using LPCVD[114]. Thanks to the gaseous form of the precursor, conformal deposition can be achieved on the 3D structure. Moreover, high purity of the deposited material can be achieved at a relatively high deposition rate. The drawbacks of these methods are on the limited precursor choices and their toxicity. CVD is also used to grow Si nanowires using a technique called vapor-liquid-solid (VLS) growth[87]. With the help of metal catalysts such as Au nanoparticles that are deposited on a Si substrate, crystalline Si nanowires can be grown. Control of the nanowire geometries can be realized by strictly tuning the process conditions.

With the increasing needs for a more versatile geometry customization, especially in 3D architectures, 3D printing has gained more attention in the past few years[60,115,116]. In particular, the employment of 3D printing for micro-LIBs enables the fabrication of free-form geometries for a wide range of materials. The method is based on ink slurry containing Si that is similar to the one used in the conventional LIBs[117]. A variation of process types is available including laser-based stereolithography, extrusion-based, or material-jetting processes. Nevertheless, the development of Si micro-LIBs fabricated by 3D printing is still in the development stage. Further understanding about the processing conditions is required and the fabrication parameters still need to be optimized before adopting this technology to a larger scale. For example, Drews et al. demonstrated the fabrication of a 3D Si anode by 3D printing and comparing different slurry contents and their impact on device performance[118]. A careful selection of ink material is needed whilst the choice is also still limited. Ultimately, this method holds a promising potential for future all-3D-printed Si-based micro-LIBs.

The other way to fabricate 3D Si anode is by a selective removal of the material, the so-called subtractive method. This method is common in semiconductor fabrication technology. Starting from a Si wafer, area-

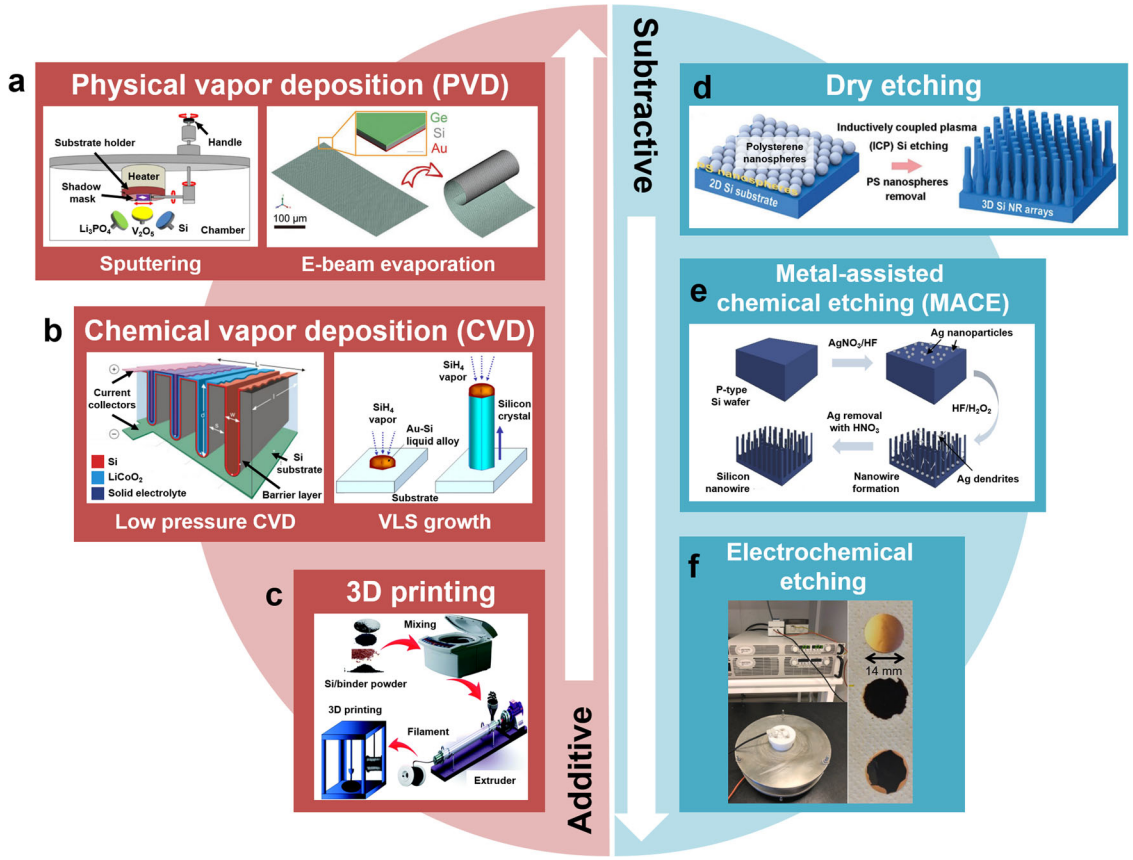

Fig. 3 | Fabrication methods of 3D Si anodes for micro-LIBs, classified as additive and subtractive techniques. Additive techniques used for fabricating Si anodes in a bottom-up manner include **a** physical vapor deposition (PVD) processes (e.g., magnetron sputtering (adapted with permission from ref. [102]. Copyright 2020 Elsevier) and electron beam evaporation (adapted with permission from ref. [89]. Copyright 2020 Wiley-VCH GmbH)), (**b**) chemical vapor deposition (CVD) processes (e.g., low pressure CVD (LPCVD) (adapted with permission from ref. [114]. Copyright 2008 Wiley-VCH GmbH) and vapor-liquid-solid (VLS) growth (adapted with permission from ref. [87]. Copyright 2008 Elsevier)), and (**c**) 3D printing (reproduced from ref. [117], https://doi.org/10.1039/D1RA06643A, under the terms of the CC BY 3.0 license https://creativecommons.org/licenses/by/3.0/). On the other hand, subtractive techniques mainly involve etching techniques (top-down) including (**d**) dry etching (adapted with permission from ref. [119]. Copyright 2020 Wiley-VCH GmbH), (**e**) metal-assisted chemical etching (MACE) (adapted with permission from ref. [126]. Copyright 2022 Wiley-VCH GmbH), and (**f**) electrochemical etching (adapted with permission from ref. [88]. Copyright 2022 Elsevier).

selective removal of the material (*i.e.*, etching) is defined by a patterning step. The deposited patterns on the Si wafer will later act as a protecting mask in the vertical etching and transfer their shapes, hence, they determine the final 3D geometry. Depending on the desired 3D shapes and dimensions, there are some reported methods to fabricate patterns (also known as lithography) for Si anodes in micro-LIB applications including photolithography and colloidal nanosphere lithography[119–121]. Hur et al. reported the fabrication of Si micropillar arrays using the combination of photolithography and deep reactive ion etching (DRIE)[66]. This type of etching is classified as dry etching because the etchant is in the form of a gas plasma. By applying a bias voltage, plasma-generated radicals and ions are bombarding the Si surface with high directionality, resulting in anisotropic etching. Since the 3D Si anode is fabricated directly from a Si wafer, the main characteristic is that the anode is made from monocrystalline Si (as compared to most additive methods where Si is deposited in amorphous form). Moreover, the 3D Si structure acts as both platform and active electrode, which makes it possible for the micro-LIB to be monolithically integrated within a chip[65]. A main limitation of this method is that the lateral dimensions of the 3D Si structure depend on the fabricated mask. In the case of photolithography, which is limited by diffraction, it is extremely difficult to fabricate a high areal density of very small structures (e.g., submicron-sized pillars) in a good resolution. Meanwhile, the application of colloidal nanosphere lithography can mitigate this restriction. However, it is challenging to fabricate a well-ordered monolayer of nanospheres on large areas, which will bring an adverse issue for wafer-scale production. Furthermore, colloidal nanosphere lithography often produces line-like defects on several areas on a chip resulting from inhomogeneously distributed monolayer nanopatterns.

Another type of etching is wet chemical etching. As the name suggests, the etching mechanism is carried out by an etchant in the form of liquid. Compared to dry etching, wet etching is a purely chemical process without a directional physical component. Here, the fabrication of 3D structure is realized by area-selective controlling the reaction rate in a certain direction. In metal-assisted chemical etching (MACE), vertical Si nanowires can be fabricated in an etching solution containing and oxidizing agent and HF by depositing metals such as Au or Ag on a Si wafer. The presence of metal catalyzes an oxidation/etching reaction at the metal-Si interface. Hence, etching occurs area-selectively and mostly in vertical direction. By defining the lateral geometry of the metal thin film prior to etching, vertical Si nanowires can be realized using MACE[122–125]. Deposition of metal in this method can be carried out either by a solution-based process (in which metals will precipitate on Si wafer as islands) or by a lift-off process involving lithography and evaporation. The former method (i.e., solution-based process) has been demonstrated by Eldona et al., where a highly dense nanowire forest was fabricated directly on a Si wafer, which was utilized as a Si anode[126]. Since the process is solution-based, it is considered to be low-cost. However, the non-ordered nature of the process gives rise to reproducibility issues. Electrochemical etching is also used to fabricate a porous Si anode[97]. The etching process is done in a wet environment using an electric current to catalyze the etching process. Zhao et al. fabricated a porous Si anode using the electrochemical technique[88]. The fabricated Si anode has a

Table 2 | Fabrication methods of 3D Si micro-LIBs

Method	Material	Advantages	Disadvantages	References
Sputtering	a-Si thin film	Wide variety of materials and substrates	High cost, low efficiency, low deposition rate, and low conformity	101,102,147,173,174
E-beam evaporation	a-Si thin film	Efficient process and possible deposition of materials with high melting point	High cost and low conformity	89
LPCVD	Poly-Si thin film	Conformal deposition, high purity, and high deposition rate	Limited material options based on the used precursors and high toxicity	114
VLS growth	c-Si nanowires	Low-cost and feasible process of very small nanostructures	Irregular nanostructures and difficult-to-control uniformity	87
3D printing	Si/C nanoparticle – graphite blend slurry	Flexible design and fabrication capability for uncommon 3D structures.	Limited choice of ink materials	117,118
Dry etching	c-Si micro-/nanopillar arrays	Highly regular structure and well-established process in industrial scale	High investment for the equipment	65,66,120,121,142,143
MACE	c-Si nanowires	High density of nanowires, low production cost, and simple process	Irregular nanowires and hazardous etching substance	125,126
Electrochemical etching	Meso-/macroporous c-Si	Low production cost, fast process, and well-controlled nanostructure geometry	High surface roughness	88,97,153

Various fabrication methods including additive and subtractive processes possess their own advantages and disadvantages.

larger surface area compared to a planar Si, introduced by the 3D porosity, which leads to an improved battery performance.

Recent emerging applications of 3D Si micro-LIB

The original idea behind the design of micro-LIBs was to make them smaller by using the same component configuration and chip area as conventional bulk batteries. In the first versions of micro-LIBs, the batteries were arranged in a sandwich-like or adjacent configuration on a single substrate. This simple and stable structure continues to be used in many thin film and all-solid-state micro-LIBs. However, to achieve higher capacity and power density in micro-LIBs, more electrode materials need to be loaded, which in turn increases the thickness of the electrode[127]. This phenomenon poses two main challenges for conventional structures. The first issue is related to the microelectrodes' kinetics. As the electrode thickness increases, the distance that ions need to travel also increases. This leads to a reduction in the driving force of the electrochemical reaction as the distance from the electrolyte increases. Consequently, the power density and electrode capacity utilization decrease[128]. The second challenge is that thick electrode materials are prone to structural limitations (e.g., film delamination)[129]. Moreover, those structures are still hindered by their limited power and energy capacity.

Nowadays, the design of micro-LIBs must cater to the specific demands of different application scenarios. For example, wearable power for smart and personalized electronics is a significant application of micro-LIBs, which necessitates excellent deformation and stress resistance[130]. To address the challenges, the use of 3D architecture in micro-LIBs can provide increased capacity and electrode surface area per unit geometric footprint. The short diffusion length of Li^+ ions in the 3D architecture facilitates their rapid transport, eliminating the dependence of capacity on ion transport[131]. In addition, the enlarged electrode/electrolyte boundary surface area prevents the decrease in driving force of electrochemical reactions due to transport effects, resulting in improved capacity utilization. Additionally, these micro-LIBs offer more surface area for electrochemical reaction sites and greater design flexibility to accommodate the expanded volume[132]. Therefore, expanding the effective surface area of electrodes is a critical aspect of micro-LIB design. By optimizing the architecture, it is possible to achieve a larger surface area and shorter ion diffusion even with thicker electrodes and more extensive mass loading. The most common 3D architectures are interdigitated electrode, vertical pillars, coaxial pillars, and Swiss-roll structures. Other structures such as microporous, interconnected-network, or hierarchical structures can also be classified as 3D structures. Figure 4 summarizes the classification of various device architectures used in 3D Si micro-LIBs. A comparison of battery performance between different Si-based micro-LIB architectures is compiled in Table 3.

Interdigitated structures

Several methods exist for creating 3D microbattery structures, including electrodeposition, inkjet, and dispenser printing. Additive manufacturing with dispenser printing is a simple and low-cost method of producing microbatteries. Furthermore, by adjusting the amount or type of specific components, the slurry formulation can be adapted from industrial battery cell production[133]. The 3D-printed batteries' energy density can be increased by depositing an active material in the *z*-direction while the cell's power density remains constant. Furthermore, interdigitated structures help to achieve that goal. This fundamental property of additively manufactured batteries increases the cell's energy density geometrically and by material. The simulation and experimental results demonstrated that the interdigitated battery design enabled by 3D printing has the potential to overcome the trade-off between energy and power densities[134]. Several non-academic teams have implemented such 3D structures in their battery prototypes and products[135]. Addionics, a UK-USA-Israel-based company that has received funding from the European Union's Horizon 2020 research and innovation program, has developed its technology in this 3D architectural design. Some researchers from A123 Systems Inc., Massachusetts Institute of Technology, registered a Chinese patent on battery structures technologies, including interdigitated structure manufacture

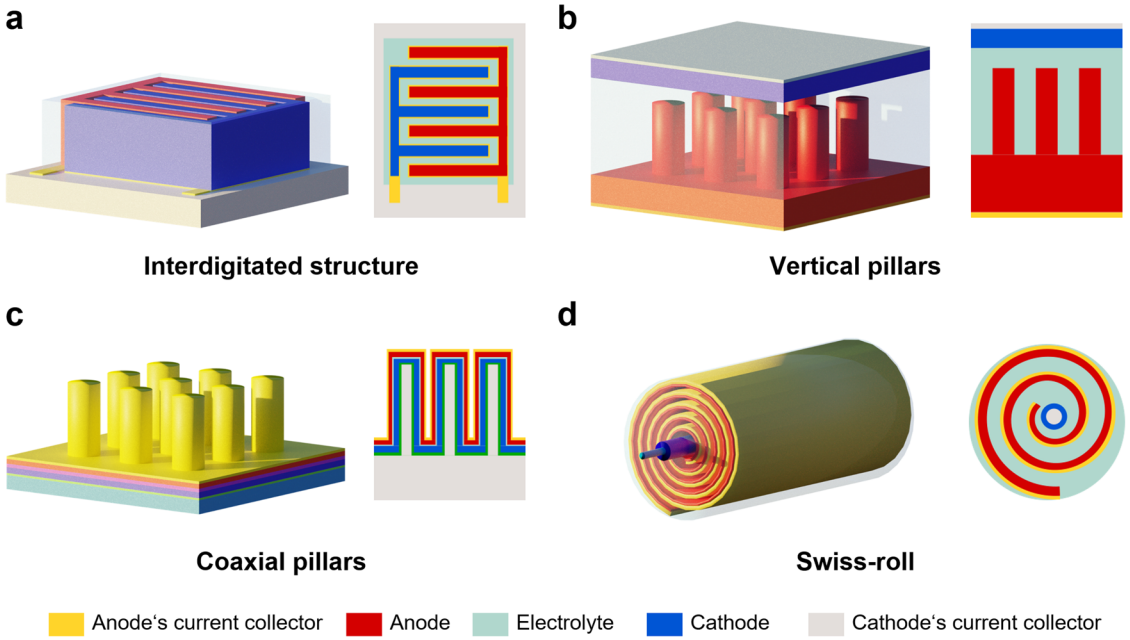

Fig. 4 | Various 3D architectures applied in Si micro-LIBs. In general, 3D architectures can be mainly classified as (**a**) interdigitated structure, (**b**) vertical pillars, (**c**) coaxial pillars, and (**d**) Swiss-roll structure.

Table 3 | Various structures of Si micro-LIBs and their performance

Architecture	Materials			Capacity		Rate capability	Capacity retention	Coulombic efficiency	Cycle	Refs.
	Anode	Electrolyte	Cathode	Areal capacity	Specific capacity					
Thin film	a-Si	LiPONB	Li metal	40 μAh cm^{-2}	-	800 μA cm^{-2}	-	99.99%	1500	101
Thin film	a-Si	LiPON	VO-LiPO	15.7 μAh cm^{-2}	-	-	49%	-	30	102
Thin film	Poly-Si	LiPON	$LiCoO_2$	-	3000 mAh g^{-1}	40 mA cm^{-2}	-	-	60	114
Interdigitated structures	Si/C-graphite	LP30/FEC	Li metal	-	466 mAh g^{-1}	2 C	75%	-	65	118
Vertical pillars	c-Si	SU-8	NCA	1.8 mAh cm^{-2}	-	0.66 mA cm^{-2}	-	92%	100	66
Vertical pillars	c-Si	$LiClO_4$	NCA	9.4 mAh cm^{-2}	-	181 mA cm^{-2}	83%	99.9%	200	65
Vertical pillars	c-Si	$LiClO_4$	Li metal	-	1093 mAh g^{-1}	-	-	98.9%	5	143
Nanowires	c-Si/PANI	$LiPF_6$	Li metal	2 mAh cm^{-2}	-	2 mA cm^{-2}	-	~100%	346	126
Nanowires	c-Si	$LiClO_4$	Li metal	3000 μAh cm^{-2}	-	35 μA cm^{-2}	43%	-	20	87
Coaxial pillars	a-Si	LiPON	$LiCoO_2$	25 μAh cm^{-2}	-	27.6 μA cm^{-2}	-	-	20	147
Coaxial pillars	c-Si /TiN/Sb	$LiPF_6$	Li metal	400 μAh cm^{-2}	-	200 μA cm^{-2}	-	~100%	500	119
Swiss-roll structures	Si-Ge	$LiPF_6$	$LiMn_2O_4$	1053 μAh cm^{-2}	-	1.04 μA cm^{-2}	67%	85%	50	89
Mesoporous	c-Si	$LiPF_6$	Li metal	-	2480 mAh g^{-1}	500 μA cm^{-2}	97%	-	70	153
Macroporous	c-Si	PVDF-HFP	$LiCoO_2$	226 μAh cm^{-2}	-	400 μA cm^{-2}	98%	99%	15	97
Honeycombs	c-Si/TiN/Ge	$LiPF_6$	$LiCoO_2$	0.15 mAh cm^{-2}	-	0.5 mA cm^{-2}	-	~100%	500	155

Comparison is made in terms of their architecture, materials, and performance metrics (i.e., capacity, rate capability, and capacity retention, Coulombic efficiency, and cycle).

technology, in 2010 (expired in 2022). On the other hand, Palo Alto Research Center Inc. has been filing US patents for its interdigitated electrode device technology since 2017.

In the case of Si micro-LIB, Drews et al. proposed customized Si/C-graphite blend slurries as anode for 3D lithium-ion micro batteries[118]. Interdigitated structures were dispensed on copper substrates to investigate the aspect ratios of 3D-printed Si/C–graphite anodes. The optimal capacity and rate performance characteristics of lithium metal cells containing 12 wt % binder were determined using a coin cell configuration. Even though the used slurries had a relatively wide particle size distribution, they could be extruded successfully and reliably through 110 mm micro nozzles available commercially without clogging. From rheological investigations (i.e., yield stress measurements), it was revealed that a higher binder content is advantageous for the dispensing process. In this regard, 3D-printed interdigitated-anode structures with higher binder concentration exhibited higher aspect ratios of up to 6.5, indicating that they hold great promise for fully printed 3D Si micro-LIBs.

Electrochemically optimized slurries have poor rheological and dispensing properties and vice versa, revealing a fundamental trade-off between electrochemical and dispensing properties. Based on this study and the given material composition, Si/C–graphite blend slurries with 18 wt% binders are recommended for use in 3D Si

micro-LIBs because they combine high capacity values (466 mAh g^{-1} at C/4) and multiple rate performance (around 427 mAh g^{-1} at 2 C) with aspect ratio values close to 6 within an 8-layered structure. Nevertheless, future research will concentrate on enhancing the printability of anodes with a lower binder content and improved electrochemical performance by using additives that increase viscosity. Carboxymethyl cellulose (CMC) and styrene–butadiene rubber (SBR) binders are a suitable systems for Si-based anodes from an electrochemical standpoint due to their ad- and cohesion-enhancing properties in the dispenser printing process.

Because of this unique design nature, the 3D current-collector architecture determines the overall cell morphology and serves as the foundation for the other cell components. This phenomenon contradicts the recent methods, which can only produce layered structures with 2D morphology, long transport lengths, and small interfacial surface areas between the electrodes. Again, an advantageous aspect of the interdigitated structure is provided by its flexible customization of the current collector architecture. A configurable architecture permits tuning the cell properties for particular applications based on performance metrics, including cost, power density, energy density, safety, and cell life[136].

Vertical pillars

The increase of surface area through 3D morphology can also be achieved by microstructuring a Si anode using subtraction methods to form vertical pillars. The fabrication of such structure is compatible with the tools that are commonly used in semiconductor processing lines (e.g., lithography and etching machines). Moreover, micro-LIBs can be fabricated on-chip, and the crystalline Si wafer can directly act as both substrate and active material for lithium storage. In general, Si vertical pillars are firstly fabricated from the Si substrate by a micropatterning process of mask material (e.g., photoresist or nanoimprint resist), followed by vertical etching[137–141]. The following procedures include the deposition of electrolyte, cathode, and lastly, current collector to complete the electrochemical cell.

The realization of a vertical-pillar-anode concept for micro-LIBs was demonstrated by Lethien et al., as shown in Fig. 5a, b[142]. They proposed a method to fabricate vertical Si pillar anodes using conventional lithography and reactive ion etching (RIE). This method has the advantage over bottom up methods (e.g., CVD), that it does not require high-temperature synthesis and long process times when long nanowires are desired, which would limit its application in industrial scale. Using low-cost photolithography, a positive photoresist was patterned to yield an array of pillars with a diameter of 500 nm and a pitch of 1 µm with great reproducibility. The photoresist acted as a mask for deep reactive ion etching (DRIE) using the so-called Bosch process. The characteristic of this process is that it introduces a scalloping shape of the nanopillar sidewalls. With an optimized process, Si nanopillar arrays with high aspect ratios of ~20 were achieved. Although it is possible to reach higher aspect ratios using such a technique, the nanopillar height was optimized at 10 µm considering the limitation of RF sputtering to form a conformal layer on high-aspect-ratio structures (compared to ALD). RF sputtering is used to deposit 2.5 µm of LiPON/$LiFePO_4$ dual layers, which act as the solid electrolyte and the cathode, respectively. The deposition using RF sputtering is highly directional and not area-selective. Therefore, a patterning technique of photoresist by means of photolithography and lift-off is used to area-selectively deposit LiPON/$LiFePO_4$. Here, the lift-off process is constrained by the solubility of LiPON in tetramethylammonium (TMAH) and acetone. Hence, avoiding the use of a photoresist removal solution containing those substances is mandatory. Moreover, high-temperature annealing is necessary to transform the amorphous $LiFePO_4$ to its crystalline form to improve Li^+ ion transport. The annealing of the LiPON/$LiFePO_4$ dual layers has to be carried out only after the lift-off process to prevent damage to the photoresist. It is reported that porous Nasicon (monoclinic structure) $Li_3Fe_2(PO_4)_3$ was formed instead of the orthorhombic crystalline $LiFePO_4$. Although Nasicon $Li_3Fe_2(PO_4)_3$ has a lower specific capacity (120 mAh g^{-1}, compared to 170 mAh g^{-1} in orthorhombic crystalline $LiFePO_4$ structure), it is still acceptable for battery operation. Despite successful fabrication of micro-LIBs with a conformally coated solid electrolyte and cathode around the vertical pillar structures, no electrochemical test was reported in this study[142].

One of the challenges of a 3D micro-LIB is the conformal deposition of the solid electrolyte. Hur et al. proposed a technique to conformally coat a Si pillar array by SU-8 photoresist using photolithography (see Fig. 5c)[66]. Compared to other techniques, which allow conformal deposition of a solid electrolyte on a 3D electrode such as ALD and electrodepostion, photolithography enables the deposition of a solid electrolyte with sufficient thickness within a relatively short time. Additionally, the conductivity of SU-8 can be altered by chemical modification. The Si vertical pillars are fabricated by photopatterning of a mask combined with DRIE, resulting in Si pillars with a diameter of 100 µm, a pitch of 200 µm, and a height of 400 µm. To deposit SU-8, photolithography is once again conducted by careful alignment of a pattern with a diameter of 20 µm larger than the pillar's. This results in a conformal coating of SU-8 on the Si pillars with a thickness of 10 µm. Moreover, the development time of SU-8 is limited, so that a 50-µm-thick SU-8 layer remains to cover the base of the Si pillars. To complete the battery, a slurry containing a mixture of NCA and graphite is deposited by drop casting to fill the gaps between SU-8/Si pillars, forming some kind of 3D cathode. This step is performed under vacuum to ensure a complete infiltration of NCA into the 3D structure by removing bubbles from the SU-8. The full 3D battery cell reaches a discharge capacity of 1.8 mAh cm^{-2} (5.2 mW cm^{-2}), twice the highest reported thin-film battery before (see Fig. 5d). At a current density of 0.66 mA cm^{-2}, the capacity reaches 0.56 mAh cm^{-2} (1.6 mWh cm^{-2}) with a Coulombic efficiency of 92% over 100 cycles. This is among the highest energy densities in literature so far. Despite the successful demonstration of a working 3D-structured battery, improvement can be expected by decreasing the diameter of Si pillars and simultaneously increasing the number of pillars (in other words, increasing the areal density of the Si pillars) to shorten the lithium-diffusion pathways. Another important note is to develop better cell packaging to overcome the volatility of the dimethyl carbonate (DMC) component in the ethylene carbonate (EC)/DMC electrolyte. Also, increasing the uniformity and packing density of the cathode can lead to a full-cell energy density of 10 mAh cm^{-2}.

Sternad et al. reported the electrochemical performance of micrometer-sized Si towers as the anode of micro-LIBs (see Fig. 5e, f)[143]. The Si tower arrays have a size of 50 × 50 $µm^2$, a height of 32 µm, and a distance between towers of 17.5 µm. The area of each micro-LIB device is 4 × 4 mm^2, fabricated using standard photolithography and DRIE from a highly doped (with boron) 8-inch, <100 > -oriented Si wafer. The shape of the base area of the towers is square, and they are crystallographically oriented so that the sidewalls are represented by {110} planes, which corresponds to the most preferred orientation for lithiation. To test the electrochemical performance of the Si tower anode, a Swagelok cell with three-electrode configuration is used. It is assembled as a half-cell with borosilicate-glass-fleece separator wetted with propylene carbonate and 1 M $LiClO_4$ as the electrolyte, and lithium metal as the counter electrode as well as the reference electrode. Cyclic voltammetry (CV) tests on the cell revealed an overvoltage at 100 mV vs. Li/Li^+ at the first cycle, indicating that the monocrystalline Si undergoes the so-called activation process, in which the closed surface of Si breaks up due to lithium insertion. As the number of cycle increases, the anode started to show electrochemical activity. From the cycling test, the Si towers exhibited 1093 mAh g^{-1} of specific capacity at a Coulombic efficiency of 98.9% for 5 cycles. The calculation of gravimetric capacity was carried out by approximating the density of Si and the evaluation of the total Si volume involved in the lithiation, determined by the lithiation depth. Using focused-ion beam (FIB) to prepare a cross-sectional view of the towers by scanning electron microscopy (SEM), it is clear that there are at least three different regions formed after 5 cycles (see Fig. 5e, f). The bottom region (region I) is the non-lithiated monocrystaline Si, which acts as the

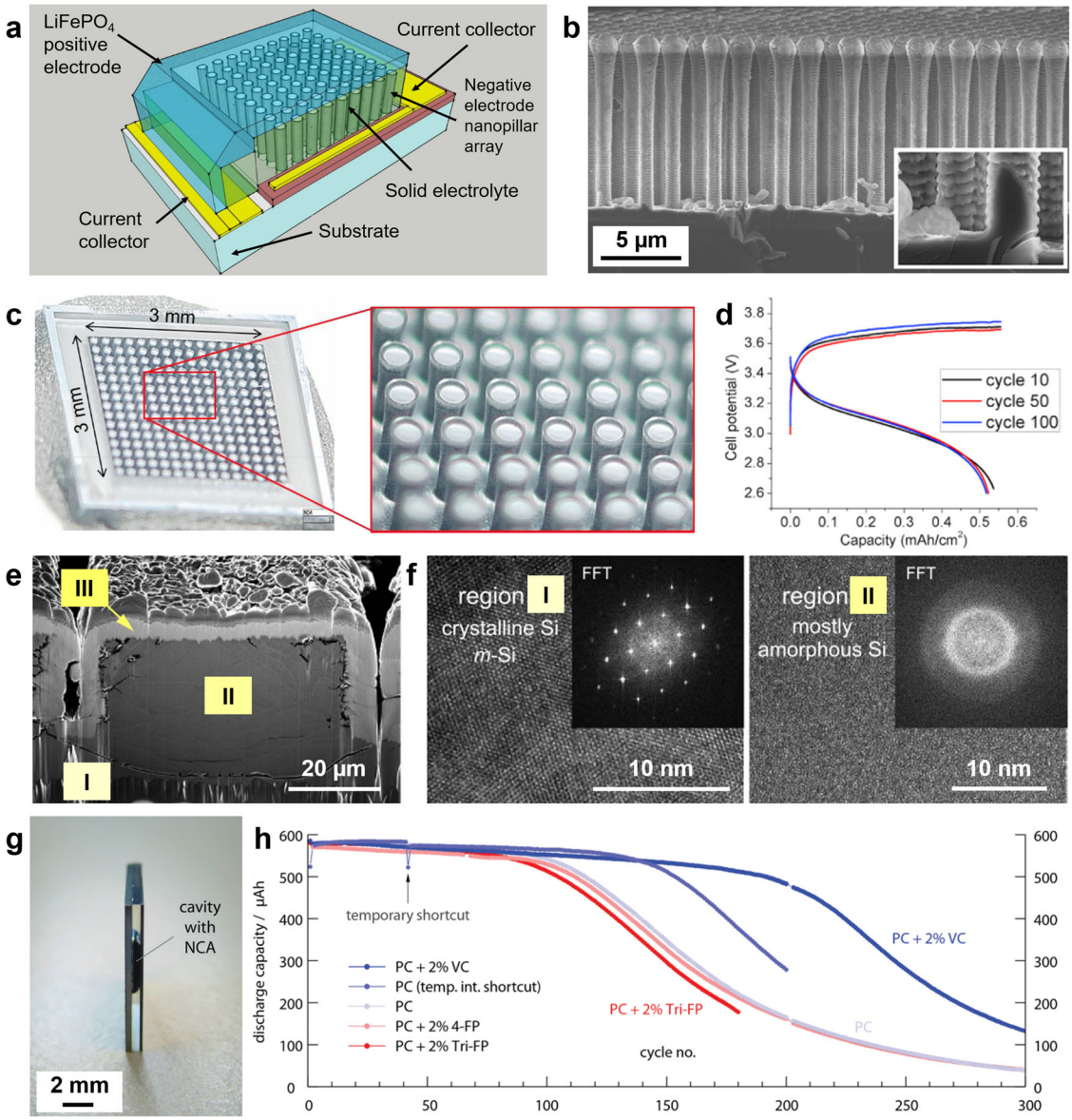

Fig. 5 | Vertical pillar structures used in 3D Si micro-LIBs. a Concept of 3D micro-LIB integrating pillar structures. **b** Si micropillars fabricated by deep reactive ion etching using the Bosch process showing scalloped sidewalls deposited by LiPON/$LiFePO_4$ dual layers. Adapted with permission from ref. [142]. Copyright 2011 Elsevier. **c** Conformal deposition of SU-8 photoresist on Si micropillars. **d** Cycling performance of SU-8 coated Si pillars, showing good capacity retention at the specific capacity of 0.56 mAh cm^{-2} with a Coulombic efficiency of 92% over 100 cycles. Adapted with permission from ref. [66]. Copyright 2018 Elsevier. **e** Cut through a Si tower by focused ion beam (FIB) showing a scanning electron microscopy (SEM) cross-sectional view. Different colors indicate different phases of lithiated Si (5 cycles). **f** Transmission electron microscopy (TEM) images of the respective phases of lithiated Si, monocrystalline Si (region I) and amorphous Si (region II). Adapted with permission from ref. [143]. Copyright 2016 Nature. **g** Side view of a 4 × 4 mm^2 micro-LIB. **h** Charge/discharge cycling performance of the monocrystalline Si micro-LIB with different electrolyte compositions. Adapted with permission from ref. [65]. Copyright 2021 Wiley-VCH GmbH.

current collector. The second region (region II), which is mostly located in the Si tower, is a mixture of amorphous Li_xSi and monocrystalline Si. A third region (region III) lying at the surface of the Si anode, corresponds to a capping layer formed as an artifact of FIB. The lithiation depth is determined as 32 µm which is the height of Si tower itself. Morphological changes of Si are also evaluated in this study. The lithiation caused a volume expansion changing the size of the Si towers up to 37% laterally and up to 31% vertically, which can be considered moderate. Obviously, Si was only partially lithiated after 5 cycles.

Further work by Sternad et al. introduces wafer-grade monocrystalline Si not only as 3D active material for lithiation but also as a housing component, as displayed in Fig. 5g[65]. They demonstrated the fabrication of a complete cell with the same areal footprint as in their previous report (i.e., 4 × 4 mm^2) but with higher Si towers (i.e., with a lateral size of 50 × 50 $µm^2$ and a height of 60 µm). A full-cell configuration was fabricated, which is mainly composed of three parts, i.e., two parts of electrode compartments (cathode and anode) and a separator. The anode part is a microstructured Si wafer (in the form of Si towers), with its backside deposited by Al as a current collector. The cathode part comprises thin Si on a glass. The glass is etched until the Si is exposed and then deposited by a polycrystalline NCA cathode material. The other side of Si is also sputtered by Al to act as the cathode's current collector. The separator is a borosilicate glass fleece, immersed in a liquid electrolyte (propylene carbonate (PC) and $LiClO_4$). To complete the cell, both the cathode and anode compartments are glued together with an ultraviolet-cured adhesive, while the wetted separator is sandwiched between them. Here, Si also acts as a packaging material that seals the whole inside of the cell. Fiber-like amorphous Si filaments draw through large areas of Si during the early stages of lithiation and activation cycles of single

crystalline Si. The in-depth lithiation occurs through a complex 3D mechanism along cracks that run preferentially along the <110> directions. High but short-term discharge currents promote surface activation and, thus, the electrochemical performance of the monocrystalline Si surface. The authors studied the impact of various additives to the electrolyte (namely, vinylene carbonate (VC), 4-fluorophenyl isocyanate (4-FP), and 2,3,4-trifluorophenyl isocyanate (Tri-FP)) to optimize the cycling performance of the cell. VC additives, which form bulky oligomeric and polymeric layers, significantly improve the cycling durability of single-crystalline Si by maintaining the capacity almost twice as good as the other additives (4-FP and Tri-FP) (see Fig. 5h). In contrast, additives that produce primarily thin inorganic SEI layers appear to have no benefit. The current Si micro-LIB can withstand more than 100 full cycles while fading capacity (only 17% after 200 cycles, 0.5 mAh, 4×4 mm^2 electrode size). At power densities as high as 100 mW cm^{-2}, the small-format system has high Coulombic efficiencies (>99.9% for the first 180 cycles) and high energy densities (30 mWh cm^{-2}). These values are equivalent to discharge densities of up to 10 mAh cm^{-2}. The high-power cell design has a power density of 200 mW cm^{-2} (energy density of 10 mWh cm^{-2}). Notably, the 3D-patterned Si anode generates very high peak discharge currents (>181 mA cm^{-2} for 1 s) comparable to dedicated state-of-the-art (large-volume) high-power cells that commonly use graphite anodes. These parameters (full-cell design) allow for an easy powering of miniaturized data-transmission devices. Importantly, all components of the microbattery are manufactured at low per-piece costs, and the design is optimized for mass production in a semiconductor manufacturing environment[65].

Coaxial pillars

Micro-LIBs with coaxial pillars have a concentric configuration where conformally deposited electrodes and solid electrolytes onto 3D arrays, result in high energy density by reducing the electrolyte volume[38,90]. The primary focus is on achieving a systematic arrangement of the electrode, the electrolyte layers, and the other electrode. Thus, by substantially increasing the loading of active components, a 3D coaxial architecture can enhance the specific capacity and energy density per unit area[144]. Moithzeim et al. fabricated 3D thin-film batteries with coaxial structure by utilizing TiO_2-coated Si micropillars[113]. A schematic of such thin-film batteries is shown in Fig. 6a. The micropillars were prepared by photolithograph patterning, followed by DRIE. The design that employs micropillar arrays with coaxial architecture is considered to mitigate the technological challenge of conformal coating, as the open and ordered structure simplifies the deposition of successive layers. The architecture of the 3D micropillar arrays coated with amorphous TiO_2 used as an anode is depicted in Fig. 6b, c.

Furthermore, ALD and spatial atomic layer deposition (S-ALD) were employed for fabricating a 3D coaxial-architecture electrode. S-ALD was chosen because this technique enables precursors, which are more effectively exposed to the surface, and at the same time can be purged significantly faster[145]. The impressive performance of this coaxial electrode demonstrates its potential as a valuable architecture for producing electrodes in 3D thin-film batteries. However, the fibrous substrate's cylindrical shape makes it challenging to implement the idea of coaxial cable energy at the sub-millimeter scale. The development of thin films over microsized fibrous substrates using CVD, PVD, or ALD is a complex task[146]. In addition, their current practical applications are limited due to their relatively inadequate cycling stability. Therefore, an effective methodology is an important topic to explore for fabricating battery components on microfibrous substrates.

The use of a Si coaxial pillar structure for micro-LIB based on a Si anode was reported by Talin et al. (Fig. 6d)[147]. They fabricated a $LiCoO_2$/LiPON/Si full-cell structure on 3D-Si conical microcollumns with a 1.6 μm base diameter, a 3.6 μm pitch, and a 4 μm height. Different Si materials were used in this micro-LIB, one acts as a 3D platform for the battery and the other serves as an active anode material. The platform was fabricated from a Si wafer. Therefore, it has crystalline structure. To prevent reaction with Li during lithiation, a 300 nm thick thermal SiO_2 layer was applied to the surface of 3D Si structure before the deposition of the Ti/Pt current collector and the following cathode/electrolyte/anode materials. A 100-nm-thick *a*-Si layer was deposited as anode material, followed by a Cu current collector. The

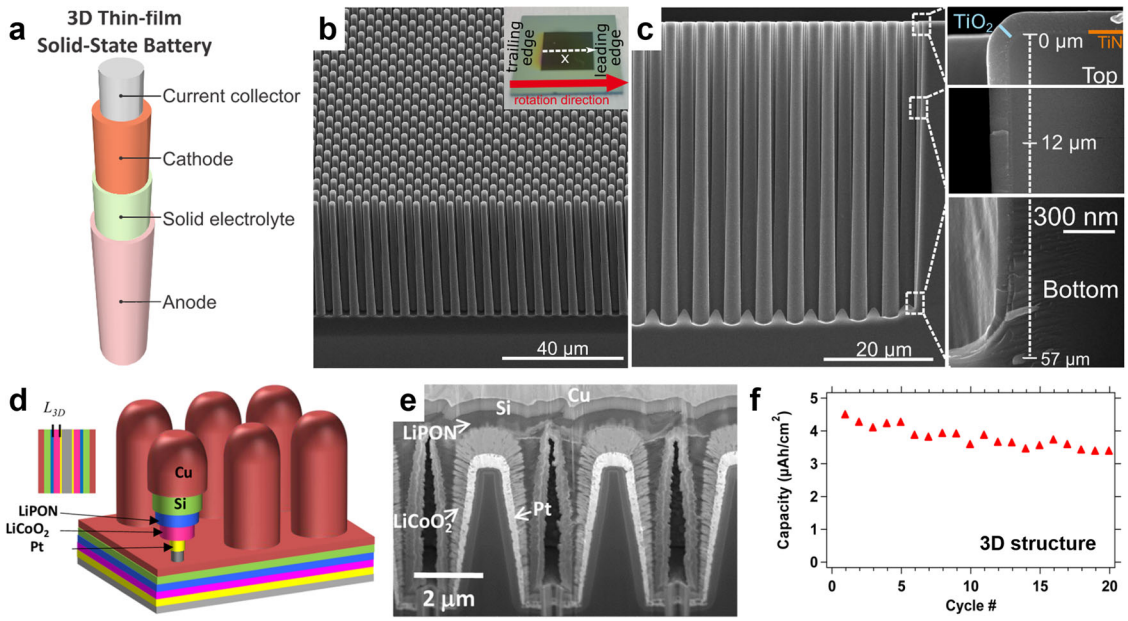

Fig. 6 | Coaxial pillar structures used in 3D Si micro-LIBs. a 3D thin-film solid-state battery showing its pillar current collector, cathode, solid electrolyte, and anode. **b**, **c** SEM images of 3D micropillar arrays coated with amorphous TiO_2 by spatial atomic layer deposition (S-ALD). Electrochemical characterization of Cl-doped a-TiO_2 films deposited on 3D substrate. Adapted with permission from ref. [113]. Copyright 2019 American Chemical Society. **d** Schematic of a coaxial pillar structure of a micro-LIB with an amorphous Si anode. **e** Cross-sectional SEM image of the fabricated coaxial pillar structure of (**d**), showing a conformal deposition of the different micro-LIB materials. **f** Cycle test of the Si micro-LIB using an amorphous Si anode in coaxial pillar configuration (**d**, **e**), indicating a degradation of capacity within 20 cycles. Adapted with permission from ref. [147]. Copyright 2016 American Chemical Society.

cross-sectional view of the structure is shown in Fig. 6e. The authors reported that the 3D coaxial-pillar structure has, surprisingly, a lower power performance compared to the planar counterparts and exhibits poor capacity retention upon cycling. Although the 3D coaxial-pillar structure has a slightly higher capacity at slow C-rate compared to its planar form (i.e., 25 μAh cm^{-2} vs. 21 μAh cm^{-2}, respectively), its capacity decreases significantly at a higher C-rate (Fig. 6f). They suggested that this lag of performance is attributed to a structural inhomogeneity (i.e., different electrolyte thicknesses that lead to nonuniform potential distribution) and low electrolyte ionic conductivity. To gain a better understanding, a finite element model of the 3D Si coaxial pillar was used to simulate its charge/discharge behavior. This simulation further confirmed that cell performance is affected by a nonuniform distance between anode and cathode as well as an impaired Li^+ transport in the electrolyte and cathode[147].

Swiss-roll structures

A micro-origami self-assembly process can convert a large-area thin film into a micrometer-sized Swiss-roll, overcoming this technological challenge. Swiss-roll fabrication follows an on-chip processing path that is compatible with the production of microelectronic devices. The method entails a thin-film self-assembly process using inherent built-in strain to form a Swiss-roll structure, mimicking the most efficient electrode design of bulk batteries.

Recently, Li et al. proposed a novel Swiss-roll microelectrodes construction[148]. Anchoring three edges of a rectangular Ti/Au sheet to a chip defines the start edge for the micro-origami process, which uses resulting hollow Swiss-rolls as microelectrodes for an on-chip battery. Two perforated Ti/Au layers are rolled against each other on a single chip to form a twin-tube architecture. Then, in order to construct a battery, electro-active materials are deposited into the Ti/Au Swiss-roll current collectors. MnO_2 and Zn are commonly used for deposition due to their high air stability. MnO_2 and Zn are successfully deposited into the Swiss-rolls, as shown by the top and side views of the tubular structures. Following a 7-minute deposition, a small amount of MnO_2 (0.8 g) is loaded onto one Swiss-roll microelectrode.

The self-assembly of thin films, aided by inherent built-in strain, results in a Swiss-roll structure that mimics the most rational electrode design for bulk batteries[148]. With a footprint area of 0.11 mm^2, the on-chip packaged Swiss-roll microbattery has a high capacity of up to 136 μAh cm^{-2} and an energy density of 181 μWh cm^{-2}. Furthermore, the on-chip fabrication procedure enables the construction of parallel battery arrays in a single manufacturing run, encouraging further development towards a new generation of microbatteries for autonomous microelectronic systems.

The Swiss-roll microbattery has a comparable energy density but costs one order of magnitude less than microbatteries with other architectures. More importantly, the cycling stability is comparable to that of the best microbatteries. By using high-capacity materials, the Swiss-roll microelectrode has the potential to achieve a higher energy density (e.g., Si, germanium).

Tang and colleagues conducted a study that utilized a Si-Ge compound to develop a fascinating microelectrode featuring a spiral architecture[89]. The spiral structure was generated by a self-assembly process driven by the internal stress in the nanomembrane's layered structure. The spiral configuration of this architecture preserves the nanomembrane's short path for charge transfer, resolving the issue of a long path for charge transfer in a thick and high-mass electrode. Finite element modeling (FEM) was used to simulate the self-assembly of a Si-Ge nanomembrane with a thickness increase factor of 1. Figure 7a demonstrates that the internal tension causes the compound nanomembrane to roll up, which has a quasi-stacked structure with an interlayer gap and nanometer thickness of each winding. As depicted in Fig. 7b, this structure will enable rapid charge transfer, eliminating the disadvantage of slow charge transport in dense microelectrodes[149].

The spiral structure of spiral microelectrode (sp-μED) displays a reversible capacity of 755 μAh cm^{-2}, indicating that it can withstand the significant volume changes in silicon and germanium without damage (Fig. 7c). The gravimetric capacity calculated from the deposited Si and Ge layers' theoretical weight is 2000 mAh g^{-1}, indicating that active materials are utilized efficiently. However, the microelectrode experienced structural fatigue and ultimately breaks down during the cycling test presumably due

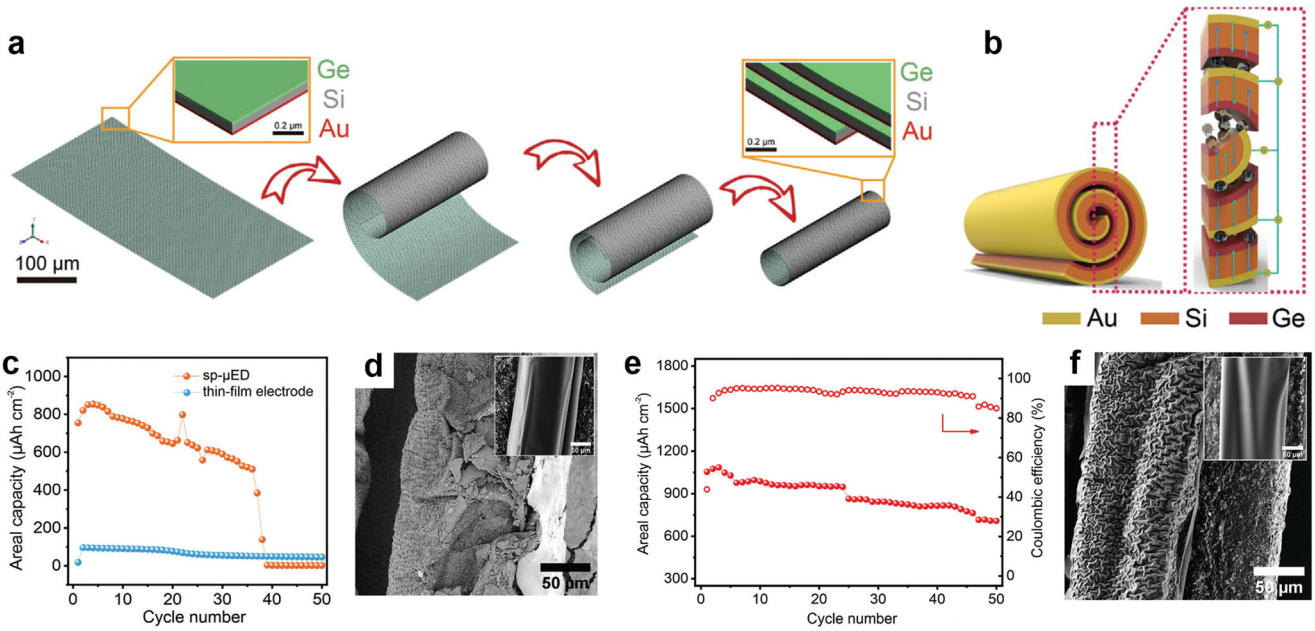

Fig. 7 | Mesostructured Swiss-roll microelectrodes used in 3D Si micro-LIBs. **a** Finite element simulation of spiral formation of a Si–Ge compound with a conductive support (Au: 5 nm, Si: 60 nm, Ge: 20 nm). **b** Schematic illustration of ion diffusion and charge-transport path in the spiral microelectrode (sp-μED). **c** Cycling stability of a Si–Ge sp-μED and a Si–Ge thin-film electrode at 9.42 μA from 0.01 to 2.5 V. **d** SEM image of a Si–Ge sp-μED after cycling; the inset shows the corresponding SEM image of the fresh electrode. **e** Cycling stability of the strengthened Si–Ge sp-μED from 0.01 to 2.5 V at 0.83 mA cm^{-2}. **f** SEM image of the strengthened Si–Ge sp-μED after cycling; the inset shows the corresponding SEM image of the fresh electrode. Adapted with permission from ref. [89]. Copyright 2020 Wiley-VCH GmbH.

to the repetitive changes in volume. As illustrated in Fig. 7d, the Si-Ge sp-μED exhibits an intact structure prior to cycling (inset). After the cycling test, the Si-Ge sp-μED fractured into multiple pieces. Since it is freestanding, the fractured Si-Ge sp-μED lost contact with the current collector, causing battery failure[150].

To prevent the cracks induced by the significant volume variations during the charge/discharge cycles, polyacrylamide (PAAm) was added as strengthening layer, which resulted in stable cycling performance. PAAm has a high level of permeability for lithium ions, which helps to preserve the exceptional energy storage capability of the Si-Ge sp-μED[151]. The maximum area capacity of the spiral microelectrode was found to be 1053 μAh cm^{-2}, and it retained 67% of its capacity after 50 cycles as shown in Fig. 7e. The wrinkled structure, as demonstrated in Fig. 7f, suggested the success of PAAm in releaving the strain caused by volumetric change during the cycling test, resulting in enhanced performance[152].

Furthermore, a spiral microelectrode served as the anode for a cylinder micro-LIB, which achieved an energy density of 12.6 mWh cm^{-3} with a volume of only 3 mm^3. In addition, the cylinder micro-LIB has a small volume and high energy density, which surpasses most current micro-LIB technologies. Thus, the current challenges faced by this spiral-architectured microelectrode are related to the developments of high-performance micro-LIBs that can be integrated into miniature electronic devices.

Other architectures

Mesoporous Si is a type of Si material that has caught the interest of researchers due to its ability to maintain stable battery cycling as its pores can accommodate the volume expansion during cycling. A Si film anode with mesoporous architecture was fabricated via electrochemical etching for micro-LIBs by Luais and coworkers[153]. A Si wafer experienced electrochemical etching, which resulted in the creation of porous Si that possesses controllable pore dimensions on a nanometer scale. Two distinct lower cut-off voltages were used during galvanostatic cycling at 300 μA cm^{-2} (see Fig. 8a). The first cut-off voltage was set at 0.1 V, which led to a steady specific capacity of 1910 mAh g^{-1} with capacity retention of 97% for 70 cycles. The second cut-off voltage was set deeper at 0.07 V, which resulted in a higher specific capacity of 2480 mAh g^{-1}. As demonstrated in Fig. 8b–d, a significant portion of the permeable layer appeared to be intact, although some of the upper layer peeled away. It is evident that mechanical reactions during the charging and discharging of the mesoporous Si anode are heavily influenced by the potential limits. It is also important to mention that the decrease in performance in this range is due to the cracking of the permeable layer and not the cracking and pulverization of the underlying Si wafer. Only the mesoporous layer of Si is engaged in the electrochemical processes of charging and discharging with lithium, while the underlying Si wafer remains unaltered even after repeated use over extended periods. Thus, mesoporous Si that is produced by electrochemical etching could serve as an effective anode material with a large capacity for micro-LIBs.

Recently, Zhao et al. also conducted a study on mesoporous Si films for anode preparation, where they used electrochemical etching with three etching parameteres to create different porous structures[88]. This study revealed that porosity and surface area of the self-standing mesoporous Si films are correlated with the reversible specific capacity and the initial Coulombic efficiency (ICE) of the films. Conversely, the cycling performance was found to be mostly influenced by the film thickness rather than pore characteristics. The highest-performing Si film anode achieved an ICE of 81.2% and maintained stable cycling for more than 450 cycles but had a specific capacity limited to 1200 mAh g^{-1} in half-cells[88].

Despite numerous published studies on porous Si anodes, so far they have not met the requirements for commercial micro-LIB applications. Mostly, there was a notable decrease in cycling performance associated with

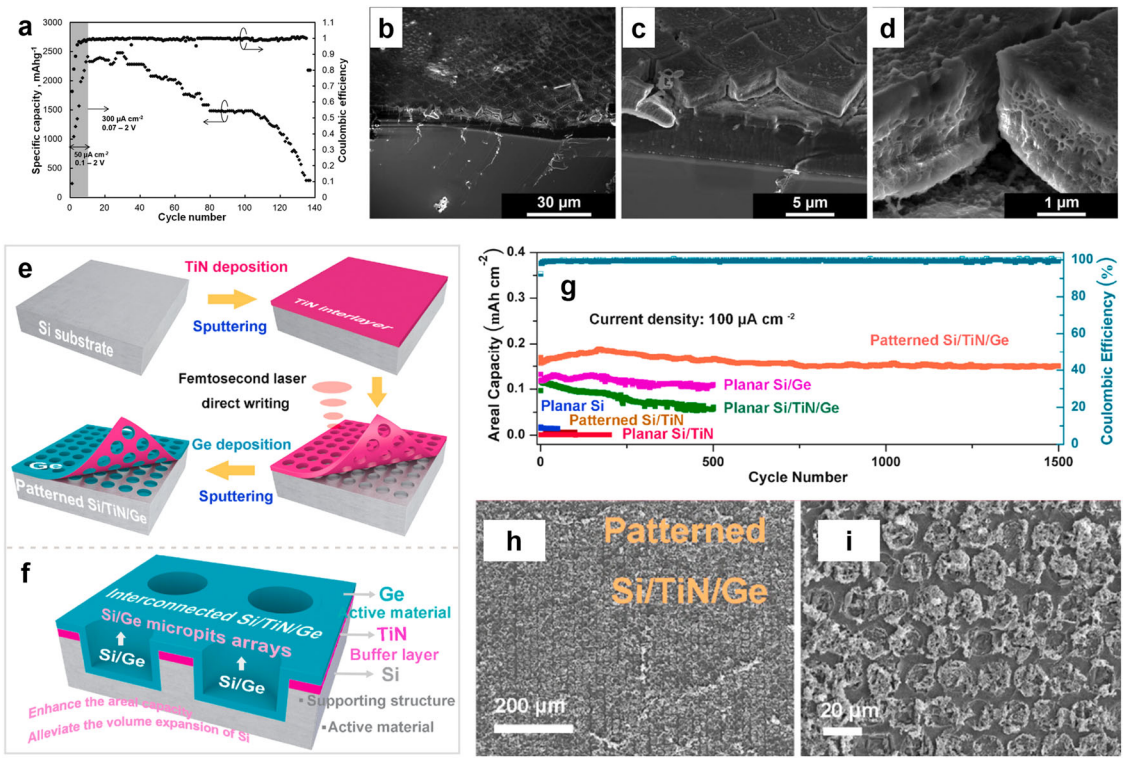

Fig. 8 | Other architectures applied for 3D Si micro-LIBs. a Galvanostatic profiles of specific capacities (diamonds) and Coulombic efficiency (circles) for a Li/*p*-type-Si half-cell with cut-off voltages of 0.07 V and 2 V. **b**–**d** SEM at different magnifications of a *p*-type Si sample after 150 galvanostatic cycles at 300 mA cm^{-2} with cut-off voltages of 0.07 V and 2 V. Adapted with permission from ref. [153]. Copyright 2015 Elsevier. **e** Illustration of the fabrication processes of the patterned Si/TiN/Ge electrode and **f** Schematic of the resuting patterned Si/TiN/Ge electrode. **g** Cycling performance of the patterned Si/TiN/Ge anode compared with those other Si-based electrodes. **h**, **i** SEM at different magnications of the post-cycling morphology of the patterned Si/TiN/Ge anode. Adapted with permission from ref. [155]. Copyright 2021 Elsevier.

a rise in specific capacity. This was caused by the creation of a crystalline alloy during charging that led to severe mechanical harm in the porous structure of the Si anode[154]. Furthermore, studying the fundamental role of Si pores in battery cycling is challenging when using composite electrodes, which often contain carbon black, extra carbon additives, and binders that can significantly improve battery performance. As such, the role of pore characteristics must be scrutinized closely. Fortunately, porous Si films can be produced without the need for carbon additives and binders, making them ideal for investigating the role of pore characteristics in a full Si anode for micro-LIB applications.

An interesting micropit honeycomb-like Si/TiN/Ge anode for stable Si-based micro-LIBs fabricated by laser micromachining was studied by Yue et al.[155]. The anode is made of a thin-film of germanium deposited via sputtering on a TiN/Si substrate, in which a micropit array of circular holes was written using fs-laser ablation, as illustrated in Fig. 8e, f. The results show that the laser-patterned Si/TiN/Ge anode provided stable cycling performance with a reversible areal capacity of 0.15 mAh cm^{-2}, which was temporarily intensified in the first 700 cycles accredited to an activation effect, before it returned back to a stable value corresponding to the initial one[156]. In addition, the anode was able to maintain 100% Coulombic efficiency even up to 1500 cycles as seen in Fig. 8g.

The use of laser patterning allows for precise control of the anode morphology, reducing the volume changes during the charge/discharge cycles and increasing its cycling stability. This architecture is beneficial thanks to the TiN layer with its micromesh pattern, which helps to gather electrons by a network of wires, through which Si and Ge are electronically connected (see Fig. 8h, i). This network serves as an advantageous buffer layer that controls the storage of Li^+ ions. Additionally, the micropit array in the Si/Ge layer can accommodate the significant changes in volume that occur in the Si substrate electrode, resulting in improved electrochemical performance[155]. This provides a promising pathway for developing high-performance micro-LIBs for use in miniaturized electronic devices.

Applicability of 3D Si micro-LIBs

The currently existing 3D Si micro-LIB designs demonstrate their potential capabilities to provide energy in different ranges of applications. The resulting areal capacities differ from tens of μAh cm^{-2} up to several mAh cm^{-2} (see Table 3). Some reports use half-cell configuration with Li metal as the counter electrode, while some other studies already demonstrate the full-cell configuration with specific cathode materials. In particular, 3D Si micro-LIBs with full-cell configurations have good performances to fulfill the requirements of integrated microelectronics, considering their operating voltages, which translate to the energy densities between μWh and mWh[112]. The thin-film structures exhibit relatively low areal capacities compared to 3D structures, for example the vertical pillar structures that have the highest areal capacity of nearly 10 mAh cm^{-2}. In terms of power, the rate capabilities that can be delivered by 3D structures are comparable to thin films, which exhibit the ability of 3D structures to provide high energy density but at the same time can be designed to produce high power density.

Amongst 3D structures, the additive-manufacturing method, which produces interdigitated structures, benefits from the flexibility of shaping the Si anode geometry. The limitation comes from the structure size determined by the nozzle diameter that is used to deposit the materials. For example, the currently demonstrated interdigitated structures possess a smallest size of several hundreds of micrometers[118]. Therefore, further miniaturization would be a challenge. In addition, the use of binder in the ink slurry obliges a fragmented Si content (i.e., Si has to be a fraction of the total mass of the anode), which might limit the areal capacity. Nevertheless, the utilization of a carbon matrix can help to maintain the structural integrity of the Si anode, hence, contributes to capacity retention. Therefore, the use of an interdigitated structure might fit to the applications in case the capacity is less important than the capacity retention. The corresponding applications might be flexible and wearable devices, where low-power electronic devices are designed to be energized by multiple charge/discharge cycles without the risk of a quick capacity degradation.

The pillar-based structures (including vertical pillars and nanowires), which are more preferably fabricated using subtractive method, offer high robustness of Si. The way these 3D structures are fabricated also enables the utilization of a monolithic Si anode without the need of any binder. Moreover, the integration of such structures into on-chip applications (e.g., microcomputers, sensors, and microrobots) can be straightforward since fabrication technologies (e.g., lithography, dry etching, and various deposition methods) are widely used in semiconductor device production. In terms of performance, the areal capacities of pillar-based structures can achieve several mAh cm^{-2}, which are relatively high compared to those of other 3D structures. It indicates that the utilization of Si can be maximized. It is also possible to exploit the high power capability due to the transformation of *c*-Si to *a*-Si, as indicated by the high rate capability of hundreds of mA cm^{-2}. The high Coulombic efficiency over hundreds of cycles makes the utilization of such 3D structures even more promising for on-chip energy storage.

The *a*-Si anodes fabricated in coaxial pillars and Swiss-roll structures are promising alternatives in semiconductor processing technology. In principle, both structure types are aimed to utilize the conformity of all micro-LIB components (i.e., current collectors, electrodes, and electrolyte) to result in a short Li^+ diffusion pathway by increasing the interfacial-area sizes within the same areal footprint. In particular, Swiss-roll structure offers a simple and low-cost fabrication method to realize this aim. The resulting rate capability is comparable with the other 3D structures. Furthermore, it has been demonstrated that the full-cell prototype of a Swiss-roll structure with an areal footprint of 0.17 mm^2 is capable of powering a digital watch for 15 min, which is normally energized by a conventional AA battery, showing its potential as an alternative for a battery power supply[89].

Applications of 3D Si micro-LIBs may also be challenged by varying operating temperatures. Unfortunately, there is still limited information provided by published sources, especially regarding the relation between temperature and structural integrity of the various 3D Si anodes. However, elevated temperatures can affect the kinetics of the battery. At elevated temperatures, the ionic conductivity of the solid electrolyte may decrease compared to a liquid electrolyte[66]. This may be an important criterion for material selection.

Research in 3D Si micro-LIBs has successfully shown the capability of various structural designs from the level of proof-of-concept up until prototyping. Indeed, the demonstrated 3D designs have exhibited promising specific capacities, rate capabilities, as well as cyclabilities. Nevertheless, the implementation of these results into commercial use might pose different challenges.

Firstly, the main challenge comes from the upscaling of the 3D Si micro-LIB fabrication process. As a roll-to-roll production has been established in the conventional LIB manufacturing, the current semiconductor processing technology should be able to accommodate mass production of micro-LIBs, too. The semiconductor industries have successfully automated large-batch production of microelectronic devices, which can deliver products with high throughput. When the process tries to integrate the production of micro-LIBs, the bottleneck might come from the fact that some steps involving the deposition of Li-containing materials have to be done inside a glovebox with low humidity and oxygen content. When manufacturing a prototype of 3D Si micro-LIBs can be carried out by human hands, the automated process has yet to be established in the current semiconductor processing line. The realization of such process is imperative to enable a higher throughput and thus lower the production cost.

Secondly, although the fabrication of 3D Si structures has already been well established for microelectronic devices, the fabrication of a complete 3D Si micro-LIB requires an optimized and reliable device performance before going to the real market. Most of the reported 3D Si micro-LIBs still show stable performance in hundreds of cycles, whereas the actual need usually necessitates a stable and reproducible battery performance in thousands of cycles. Bridging this gap can be accomplished by pushing more research not only to a proof-of-concept, but further to the long-term reliability of 3D Si micro-LIBs. In fact, the published results, specifically about the utilizations

of 3D Si anodes for micro-LIBs, are still very limited. This is in contrast with the results of nanostructured Si anodes for conventional LIBs.

Lastly, while many studies on 3D Si micro-LIBs focus on the development of performance metrics, there are still a few that are dedicated to include the packaging aspect. Packaging is a final step in 3D Si micro-LIB fabrication that requires special attention since it is related not only to performance aspects such as reliability of the device, but also safety issues. In general micro-LIB research, efforts are directed towards the utilization of solid electrolytes since the application of micro-LIB has to be compatible with solid-state electronics. Packaging for such type of electrolytes (e.g., LiPONB and SU-8) in 3D Si micro-LIB has been done for example by epoxy encapsulations[66,101]. Liquid electrolytes, which are used in 3D Si micro-LIBs such as $LiClO_4$ or $LiPF_6$, are mostly used in half-cell configurations resulting in packaging forms of Swagelok cells or CR2032 coin cells[87,118,119,126,143,153,155]. However, some of the demonstrated full-cell prototypes using liquid electrolytes have already applied packaging techniques such as the employment of sandwiched *c*-Si/glass/*c*-Si glued with UV-cured adhesive[65] or capillary tubes sealed with photocurable epoxy[89]. The scarcity of the reported packaging techniques in 3D Si micro-LIB fabrication should drive more studies about this crucial yet unexplored aspect in the future.

Conclusions and outlook

The development of portable electronics requires miniaturized energy storage devices with sufficient energy density and reasonable size. Miniaturized LIBs, or the so-called micro-LIBs, can answer the needs. The development of micro-LIBs has been carried out for a couple of decades. However, there are still many rooms for improvements in terms of performance and production techniques. At the same time, Si emerges from the conventional LIB research as a high capacity anode, although several drawbacks exist rooting from an extreme volume expansion during lithiation, which inhibit the widespread use of Si anodes so far. However, Si is often utilized as a substrate since the ultimate goal of micro-LIB development is an integrated power source directly on-chip. Moreover, processing of Si is already well-matured in semiconductor processing lines. Due to these reasons, the incorporation of Si as an anode for micro-LIBs holds many prospects. Furthermore, there are many reports related to 3D Si anode fabrication techniques, which stem from the need to, both, increase surface area and to cut the transport distance of Li^+ ions, with the aim of increasing energy and power density, simultaneously. Various 3D structures have been reported, in which interdigitated, vertical pillar, coaxial pillar, and Swiss-roll structures are the most used architectures. Each architecture has its own advantages and drawbacks compared to the others, particularly, in terms of complexity of fabrication and the possibility to scale up the production. In general, the performance of Si micro-LIBs is competetive to that of conventional LIBs, especially when applied to small footprint areas. Since the incorporation of Si as the anode for micro-LIBs is still in the developing phase, future research should be aimed at different directions.

Firstly, exploration should be further conducted on more cathode and electrolyte materials suitable for Si anodes and their deposition methods. At present, the application of various cathode and electrolyte materials for Si micro-LIB is constrained by the methods that are available in industrial semiconductor processing lines. There is a growing need to investigate the synergies and compatibilities of these newer electrolyte solutions with existing semiconductor processes. Recently, material science breakthroughs have unveiled the potential of room-temperature solid-state electrolytes, such as LLZO, LATP, and LGPS[157]. These developments promise significantly enhanced safety and performance due to their inherent stability and potential for higher energy densities of micro-LIBs. Furthermore, new liquid high-voltage electrolytes are being explored, which can further push the boundaries of energy density and extend the lifespan of the battery by reducing degradation at high voltages[158–160]. From the cathode side, the incorporation of materials with higher nickel content (e.g., $LiNi_{0.8}Mn_{0.1}Co_{0.1}O_2$ (NCM-811) and $LiNi_{0.9}Mn_{0.05}Co_{0.05}O_2$ (NCM-955)), and other potential cathode materials (e.g., $LiNiO_2$) pose great promises due to their demonstrated energy densities[81,82]. The investigation of these other types of materials that are available with the existing methods would open new paths towards higher performance and more stable Si micro-LIBs.

Secondly, a further miniaturization of the 3D Si anode geometry should be established. The current dimensions of 3D Si anodes in micro-LIBs are mostly in micrometer scale. However, the potential of nanoscale 3D Si to improve the micro-LIB performance is huge. At the moment, the required energy for integrated microelectronics with the areal footprint in the order of millimeters is within the range of μWh to mWh[112], while the devices commonly operate in the power range of nW to mW[161]. Reducing the structure of a Si anode to the nanometer scale may pack more accessible storage sites within the same areal footprint and at the same time improve the kinetics. This can enable 3D Si micro-LIB with higher energy and power density. Moreover, structural degradation of Si can be suppressed only in nanostructured Si, which can lead to better cycling stability as demonstrated in many studies[162,163]. Indeed, there are some challenges in the adoption of Si nanostructures for large scale applications such as the complexity of fabrication technique, the potentially increased cost, and the possibly reduced homogeneity. Therefore, further studies need to also consider those issues in the development of nanostructured Si anodes for microbatteries. Anyhow, improving the energy and power of microbatteries by further miniaturization of Si anode structures is not only aimed to the existing microelectronic uses, but also would potentially trigger the opening of entirely new applications.

Thirdly, the development of standard complete-cell fabrication and testing methods for micro-LIBs should be followed up. Differentiating from conventional LIBs that are usually fabricated as a coin cell and tested in a suitable electrochemical test setup, micro-LIB fabrication is based on the semiconductor processing technology, which is not directly compatible for the conventional and widely-used measurement methods. In terms of 3D Si fabrication for large-scale production, an alternative manufacturing method of femtosecond-laser ablation has yet to be more explored. Nevertheless, the use of this method to fabricate Si nano-/microstructures has been applied in many fields such as solar cells, sensors, optical detectors, and LIBs[155,164–168]. This method offers high convenience and efficiency that can potentially lower the per-piece production cost of an LIB. The deployment of femtosecond-laser ablation in 3D Si micro-LIB fabrication can be directed towards the engraving of a planar Si anode to form 3D periodic nano-/microstructures. The versatility of this method to form a wide variety of shapes can enable quick, cost-effective, large-area processing of 3D Si anodes. Moreover, when the devices shall be made as products, they have to be verified in a standard industry setup. Although some efforts to build prototypes of complete micro-LIBs and their electrochemical tests have been well-demonstrated, there are still no standardized protocols to fabricate and test micro-LIBs. The formulation of best-practice guides could enable more comparable performance metrics, which in turn will drive and accelerate the study of micro-LIBs forward.

Fourthly, monolithic integration with other devices should be demonstrated in terms of proof-of-concepts. As the goal of developing micro-LIB is to enable on-chip and portable use, it is also imperative to demonstrate the ability to fabricate both functional devices (e.g., sensors, MEMS, or other microelectronic devices) and a micro-LIB in a single chip. Only if the performance of exemplary autarkic micro-/nano systems (e.g., in wireless sensing networks) has been proven, upscaling and commercialization of micro-LIBs will get going.

Received: 2 August 2023; Accepted: 15 February 2024;
Published online: 28 February 2024

References

1. Roy, K., Lee, J. E. Y. & Lee, C. Thin-film PMUTs: a review of over 40 years of research. *Microsyst. Nanoeng.* **9**, 1–17 (2023).
2. Yang, Q. et al. Ecoresorbable and bioresorbable microelectromechanical systems. *Nat. Electron.* **5**, 526–538 (2022).
3. Quack, N. et al. Integrated silicon photonic MEMS. *Microsyst. Nanoeng.* **9**, 1–22 (2023).

4. Nikfarjam, H., Megdadi, M., Okour, M., Pourkamali, S. & Alsaleem, F. Energy efficient integrated MEMS neural network for simultaneous sensing and computing. *Commun. Eng.* **2**, 1–10 (2023).
5. Kim, J. et al. Skin-interfaced wireless biosensors for perinatal and paediatric health. *Nat. Rev. Bioeng*. 1–17 (2023).
6. Nurputra, D. K. et al. Fast and noninvasive electronic nose for sniffing out COVID-19 based on exhaled breath-print recognition. *npj Digit. Med.* **5**, 1–17 (2022).
7. Putri, L. A. et al. Rapid analysis of meat floss origin using a supervised machine learning-based electronic nose towards food authentication. *npj Sci. Food* **7**, 1–15 (2023).
8. Wasisto, H. S., Prades, J. D., Gülink, J. & Waag, A. Beyond solid-state lighting: Miniaturization, hybrid integration, and applications of GaN nano-and micro-LEDs. *Appl. Phys. Rev*. **6**, 041315 (2019).
9. Xia, Q. et al. All-Solid-State Thin Film Lithium/Lithium-ion microbatteries for powering the internet of things. *Adv. Mater.* **35**, 2200538 (2022).
10. Sha, M., Zhao, H. & Lei, Y. Updated insights into 3D architecture electrodes for micropower sources. *Adv. Mater.* **33**, 2103304 (2021).
11. Nasreldin, M., de Mulatier, S., Delattre, R., Ramuz, M. & Djenizian, T. Flexible and stretchable microbatteries for wearable technologies. *Adv. Mater. Technol.* **5**, 1–21 (2020).
12. Ni, J. & Li, L. Self-supported 3D array electrodes for sodium microbatteries. *Adv. Funct. Mater.* **28**, 1704880 (2018).
13. Harper, G. et al. Recycling lithium-ion batteries from electric vehicles. *Nature* **575**, 75–86 (2019).
14. Deng, J., Bae, C., Marcicki, J., Masias, A. & Miller, T. Safety modelling and testing of lithium-ion batteries in electrified vehicles. *Nat. Energy* **3**, 261–266 (2018).
15. Wang, C. Y. et al. Fast charging of energy-dense lithium-ion batteries. *Nature* **611**, 485–490 (2022).
16. Jetybayeva, A., Uzakbaiuly, B., Mukanova, A., Myung, S. T. & Bakenov, Z. Recent advancements in solid electrolytes integrated into all-solid-state 2D and 3D lithium-ion microbatteries. *J. Mater. Chem. A* **9**, 15140–15178 (2021).
17. Sheil, R. & Chang, J. P. Synthesis and integration of thin film solid state electrolytes for 3D Li-ion microbatteries. *J. Vac. Sci. Technol. A* **38**, 032411 (2020).
18. Wang, Z., Ni, J., Li, L. & Lu, J. Theoretical simulation and modeling of three-dimensional batteries. *Cell Rep. Phys. Sci.* **1**, 100078 (2020).
19. Hung, C. H., Huynh, P., Teo, K. & Cobb, C. L. Are three-dimensional batteries beneficial? Analyzing historical data to elucidate performance advantages. *ACS Energy Lett.* **8**, 296–305 (2023).
20. Liang, C. C. & Bro, P. A high-voltage, solid-state battery system: I. Design considerations. *J. Electrochem. Soc.* **116**, 1322 (1969).
21. Nakano, H. et al. All-solid-state micro lithium-ion batteries fabricated by using dry polymer electrolyte with micro-phase separation structure. *Electrochem. Commun.* **9**, 2013–2017 (2007).
22. Long, J. W., Dunn, B., Rolison, D. R. & White, H. S. 3D architectures for batteries and electrodes. *Adv. Energy Mater.* **10**, 1–6 (2020).
23. Zheng, S., Shi, X., Das, P., Wu, Z. S. & Bao, X. The road towards planar microbatteries and micro-supercapacitors: from 2D to 3D device geometries. *Adv. Mater.* **31**, 1–24 (2019).
24. Moitzheim, S., Put, B. & Vereecken, P. M. Advances in 3D thin-film Li-Ion Batteries. *Adv. Mater. Interfaces* **6**, 1–17 (2019).
25. Zhu, S., Sheng, J., Ni, J. & Li, Y. 3D vertical arrays of nanomaterials for microscaled energy storage devices. *Acc. Mater. Res.* **2**, 1215–1226 (2021).
26. Sun, P., Li, X., Shao, J. & Braun, P. V. High-performance packaged 3D lithium-ion microbatteries fabricated using imprint lithography. *Adv. Mater.* **33**, 2006229 (2021).
27. Wei, W. et al. High energy and power density TiO2 nanotube electrodes for 3D Li-ion microbatteries. *J. Mater. Chem. A* **1**, 8160–8169 (2013).
28. Li, J. et al. Phase evolution of conversion-type electrode for lithium ion batteries. *Nat. Commun.* **10**, 1–10 (2019).
29. Ni, J. et al. Rooting binder-free tin nanoarrays into copper substrate via tin-copper alloying for robust energy storage. *Nat. Commun.* **11**, 1–8 (2020).
30. Huo, H. & Janek, J. Silicon as emerging anode in solid-state batteries. *ACS Energy Lett*. 4005–4016 (2022).
31. Zhao, X. & Lehto, V. P. Challenges and prospects of nanosized silicon anodes in lithium-ion batteries. *Nanotechnology* **32**, 042002 (2021).
32. Li, P., Kim, H., Myung, S. T. & Sun, Y. K. Diverting exploration of silicon anode into practical way: a review focused on silicon-graphite composite for lithium ion batteries. *Energy Storage Mater.* **35**, 550–576 (2021).
33. Yuda, A. P., Koraag, P. Y. E., Iskandar, F., Wasisto, H. S. & Sumboja, A. Advances of top-down synthesis approach for high-performance silicon anodes in Li-ion batteries. *J. Mater. Chem. A* **9**, 18906–18926 (2021).
34. Balqis, F. et al. Conductive polymer frameworks in silicon anodes for advanced lithium-ion batteries. *ACS Appl. Polym. Mater.* **5**, 4933–4952 (2023).
35. Chen, M. et al. Boron-doped porous Si anode materials with high initial coulombic efficiency and long cycling stability. *J. Mater. Chem. A* **6**, 3022–3027 (2018).
36. Ren, Y. et al. Boron-doped spherical hollow-porous silicon local lattice expansion toward a high-performance lithium-ion-battery anode. *Inorg. Chem.* **58**, 4592–4599 (2019).
37. Li, Y. et al. On-chip batteries for dust-sized computers. *Adv. Energy Mater.* **12**, 2103641 (2022).
38. Hu, B. & Wang, X. Advances in micro lithium-ion batteries for on-chip and wearable applications. *J. Micromech. Microeng.* **31**, 114002 (2021).
39. Goldman, J. L., Long, B. R., Gewirth, A. A. & Nuzzo, R. G. Strain anisotropies and self-limiting capacities in single-crystalline 3D silicon microstructures: Models for high energy density lithium-ion battery anodes. *Adv. Funct. Mater.* **21**, 2412–2422 (2011).
40. Lee, S. W., McDowell, M. T., Choi, J. W. & Cui, Y. Anomalous shape changes of silicon nanopillars by electrochemical lithiation. *Nano Lett* **11**, 3034–3039 (2011).
41. Jung, H., Lee, M., Yeo, B. C., Lee, K. R. & Han, S. S. Atomistic observation of the lithiation and delithiation behaviors of silicon nanowires using reactive molecular dynamics simulations. *J. Phys. Chem. C* **119**, 3447–3455 (2015).
42. Liu, X. H. et al. In situ atomic-scale imaging of electrochemical lithiation in silicon. *Nat. Nanotechnol.* **7**, 749–756 (2012).
43. McDowell, M. T. et al. In situ TEM of two-phase lithiation of amorphous silicon nanospheres. *Nano Lett.* **13**, 758–764 (2013).
44. Goodenough, J. B. Cathode materials: a personal perspective. *J. Power Sour.* **174**, 996–1000 (2007).
45. Nitta, N., Wu, F., Lee, J. T. & Yushin, G. Li-ion battery materials: Present and future. *Mater. Today* **18**, 252–264 (2015).
46. Seong, W. M. & Manthiram, A. Complementary effects of Mg and Cu incorporation in stabilizing the Cobalt-Free LiNiO2Cathode for Lithium-Ion Batteries. *ACS Appl. Mater. Interfaces* **12**, 43653–43664 (2020).
47. Yang, G. F., Song, K. Y. & Joo, S. K. Ultra-thick Li-ion battery electrodes using different cell size of metal foam current collectors. *RSC Adv.* **5**, 16702–16706 (2015).
48. Lai, W. et al. Ultrahigh-energy-density microbatteries enabled by new electrode architecture and micropackaging design. *Adv. Mater.* **22**, E139–E144 (2010).
49. Wang, X. et al. High areal capacity Li ion battery anode based on thick mesoporous Co3O4 nanosheet networks. *Nano Energy* **5**, 91–96 (2014).

50. Porcher, W., Lestriez, B., Jouanneau, S. & Guyomard, D. Design of aqueous processed thick LiFePO4 Composite electrodes for high-energy lithium battery. *J. Electrochem. Soc.* **156**, A133 (2009).
51. Singh, M., Kaiser, J. & Hahn, H. Thick electrodes for high energy lithium ion batteries. *J. Electrochem. Soc.* **162**, A1196–A1201 (2015).
52. Jiang, F. & Peng, P. Elucidating the performance limitations of lithium-ion batteries due to species and charge transport through five characteristic parameters. *Sci. Rep.* **6**, 1–18 (2016).
53. Zheng, H., Li, J., Song, X., Liu, G. & Battaglia, V. S. A comprehensive understanding of electrode thickness effects on the electrochemical performances of Li-ion battery cathodes. *Electrochim. Acta* **71**, 258–265 (2012).
54. Zhao, R., Liu, J. & Gu, J. The effects of electrode thickness on the electrochemical and thermal characteristics of lithium ion battery. *Appl. Energy* **139**, 220–229 (2015).
55. Sander, J. S., Erb, R. M., Li, L., Gurijala, A. & Chiang, Y. M. High-performance battery electrodes via magnetic templating. *Nat. Energy* **1**, 1–7 (2016).
56. Prosser, J. H., Brugarolas, T., Lee, S., Nolte, A. J. & Lee, D. Avoiding cracks in nanoparticle films. *Nano Lett.* **12**, 5287–5291 (2012).
57. Lv, D. et al. High energy density lithium-sulfur batteries: challenges of thick sulfur cathodes. *Adv. Energy Mater.* **5**, 1402290 (2015).
58. Ceder, G. et al. Identification of cathode materials for lithium batteries guided by first-principles calculations. *Nature* **392**, 694–696 (1998).
59. Shaijumon, M. M. et al. Nanoarchitectured 3D cathodes for Li-ion microbatteries. *Adv. Mater.* **22**, 4978–4981 (2010).
60. Sun, K. et al. 3D printing of interdigitated Li-ion microbattery architectures. *Adv. Mater.* **25**, 4539–4543 (2013).
61. Zhang, S. M., Zhang, J. X., Xu, S. J., Yuan, X. J. & He, B. C. Li ion diffusivity and electrochemical properties of FePO4 nanoparticles acted directly as cathode materials in lithium ion rechargeable batteries. *Electrochim. Acta* **88**, 287–293 (2013).
62. Zhang, J. et al. High-performance lithium iron phosphate with phosphorus-doped carbon layers for lithium ion batteries. *J. Mater. Chem. A* **3**, 2043–2049 (2015).
63. Gao, C., Zhou, J., Liu, G. & Wang, L. Lithium-ions diffusion kinetic in LiFePO4/carbon nanoparticles synthesized by microwave plasma chemical vapor deposition for lithium-ion batteries. *Appl. Surf. Sci.* **433**, 35–44 (2018).
64. Gao, Y., Xiong, K., Zhang, H. & Zhu, B. Effect of Ru doping on the properties of LiFePO4/C cathode materials for lithium-ion batteries. *ACS Omega* **6**, 14122–14129 (2021).
65. Sternad, M. et al. A Lithium-Silicon Microbattery with Anode and Housing Directly Made from Semiconductor Grade Monocrystalline Si. *Adv. Mater. Technol*. 2100405 (2021).
66. Hur, J. I., Smith, L. C. & Dunn, B. High areal energy density 3D lithium-ion microbatteries. *Joule* **2**, 1187–1201 (2018).
67. Li, W. et al. High-power lithium-ion microbatteries from imprinted 3D electrodes of sub-10 nm LiMn2O4/Li4Ti5O12 nanocrystals and a copolymer gel electrolyte. *Nano Energy* **52**, 431–440 (2018).
68. Labyedh, N., Mattelaer, F., Detavernier, C. & Vereecken, P. M. 3D LiMn2O4 thin-film electrodes for high rate all solid-state lithium and Li-ion microbatteries. *J. Mater. Chem. A* **7**, 18996–19007 (2019).
69. Tesfamhret, Y., Liu, H., Chai, Z., Berg, E. & Younesi, R. On the manganese dissolution process from LiMn2O4 cathode materials. *ChemElectroChem* **8**, 1516–1523 (2021).
70. Zhu, L., Bao, C., Xie, L., Yang, X. & Cao, X. Review of synthesis and structural optimization of LiNi1/3Co1/3 Mn1/3O2 cathode materials for lithium-ion batteries applications. *J. Alloys Compd.* **831**, 154864 (2020).
71. Omar, N. et al. Assessment of performance of lithium iron phosphate oxide, nickel manganese cobalt oxide and nickel cobalt aluminum oxide based cells for using in plug-in battery electric vehicle applications. In *2011 IEEE Vehicle Power and Propulsion Conference, VPPC 2011* 1–7 (2011).
72. Yabuuchi, N. & Ohzuku, T. Novel lithium insertion material of LiCo1/3Ni1/3Mn1/3O2 for advanced lithium-ion batteries. *J. Power Sour.* 119, 171–174 2003.
73. Rakebrandt, J. H., Smyrek, P., Zheng, Y., Seifert, H. J. & Pfleging, W. Laser micro structuring of composite Li(Ni0.6Mn0.2Co0.2)O2 cathode layersfor lithium-ion batteries. In *Conference Program Digest – 7th International Conference on Manipulation, Manufacturing and Measurement on the Nanoscale, IEEE 3M-NANO 2017* 2018-Janua 57–60 (Institute of Electrical and Electronics Engineers Inc., 2018).
74. Muruganantham, R., Sivakumar, M. & Subadevi, R. Synthesis and electrochemical characterization of olivine-type lithium iron phosphate cathode materials via different techniques. *Ionics* **22**, 1557–1565 (2016).
75. Xia, H. et al. Facile synthesis of chain-like LiCoO2 nanowire arrays as three-dimensional cathode for microbatteries. *NPG Asia Mater* **6**, e126 (2014).
76. Padhi, A. K., Nanjundaswamy, K. S., Masquelier, C., Okada, S. & Goodenough, J. B. Effect of structure on the Fe^{3+} / Fe^{2+} redox couple in iron phosphates. *J. Electrochem. Soc.* **144**, 1609–1613 (1997).
77. Kim, S. et al. First-principles study of lithium cobalt spinel oxides: correlating structure and electrochemistry. *ACS Appl. Mater. Interfaces* **10**, 13479–13490 (2018).
78. Rossen, E., Reimers, J. N. & Dahn, J. R. Synthesis and electrochemistry of spinel LTLiCoO2. *Solid State Ionics* **62**, 53–60 (1993).
79. Jo, E. et al. Different thermal degradation mechanisms: role of aluminum in Ni-rich layered cathode materials. *Nano Energy* **78**, 105367 (2020).
80. Marincaş, A. H., Goga, F., Dorneanu, S. A. & Ilea, P. Review on synthesis methods to obtain LiMn2O4-based cathode materials for Li-ion batteries. *J. Solid State Electrochem.* **24**, 473–497 (2020).
81. Liu, Y., Harlow, J. & Dahn, J. Microstructural observations of "single crystal" positive electrode materials before and after long term cycling by cross-section scanning electron microscopy. *J. Electrochem. Soc.* **167**, 020512 (2020).
82. Liu, Y. et al. Impact of shell composition, thickness and heating temperature on the performance of Nickel-Rich Cobalt-Free core-shell materials. *J. Electrochem. Soc.* **167**, 160556 (2020).
83. Liu, L. et al. Layered ternary metal oxides: performance degradation mechanisms as cathodes, and design strategies for high-performance batteries. *Progress Mater. Sci.* **111**, 100655 (2020).
84. Lipson, A. L. et al. Stabilizing NMC 811 Li-Ion battery cathode through a rapid coprecipitation process. *ACS Appl. Energy Mater* **4**, 1972–1977 (2021).
85. Wu, C. Y., Bao, Q., Tsai, Y. T. & Duh, J. G. Tuning (003) interplanar space by boric acid co-sintering to enhance Li+ storage and transfer in Li(Ni0.8Co0.1Mn0.1)O2 cathode. *J. Alloys Compd.* **865**, 158806 (2021).
86. Meng, X. Atomic and molecular layer deposition in pursuing better batteries. *J. Mater. Res.* **36**, 2–25 (2021).
87. Laïk, B. et al. Silicon nanowires as negative electrode for lithium-ion microbatteries. *Electrochim. Acta* **53**, 5528–5532 (2008).
88. Zhao, X., Kalidas, N. & Lehto, V. P. Self-standing mesoporous Si films as anodes for lithium-ion microbatteries. *J. Power Sour.* **529**, 231269 (2022).
89. Tang, H. et al. Stress-actuated spiral microelectrode for high-performance lithium-ion microbatteries. *Small* **16**, 2002410 (2020).
90. Wang, Z. et al. Miniaturized lithium-ion batteries for on-chip energy storage. *Nanoscale Adv.* **4**, 4237–4257 (2022).

91. Lin, H., Noguchi, H. & Uosaki, K. Effects of HF on the lithiation behavior of the silicon anode in LiPF6 organic electrolyte solution. *ACS Omega* **5**, 2081–2087 (2020).
92. Sun, Y. et al. Development and challenge of advanced nonaqueous sodium ion batteries. *EnergyChem* **2**, 100031 (2020).
93. Wang, L. et al. Development and challenges of functional electrolytes for high-performance lithium–sulfur batteries. *Adv. Funct. Mater*. **28**, 1800919 (2018).
94. Kim, J. G. et al. A review of lithium and non-lithium based solid state batteries. *J. Power Sour.* **282**, 299–322 (2015).
95. Schnell, J. et al. All-solid-state lithium-ion and lithium metal batteries – paving the way to large-scale production. *J. Power Sour.* **382**, 160–175 (2018).
96. Chen, Y. et al. Recent progress in all-solid-state lithium batteries: the emerging strategies for advanced electrolytes and their interfaces. *Energy Storage Mater.* **31**, 401–433 (2020).
97. Chaudoy, V. et al. Anodes based on porous silicon films using polymer electrolyte for lithium-ion microbatteries. *ECS Meet. Abstr.* **MA2015-01**, 26–26 (2015).
98. Chaudoy, V. et al. Rechargeable thin-film lithium microbattery using a quasi-solid-state polymer electrolyte. *Batter. Supercaps* **4**, 1351–1362 (2021).
99. Zhang, Z. et al. 3D glass fiber cloth reinforced polymer electrolyte for solid-state lithium metal batteries. *J. Memb. Sci.* **621**, 118940 (2021).
100. Vu, A., Qian, Y. & Stein, A. Porous electrode materials for lithium-ion batteries-how to prepare them and what makes them special. *Adv. Energy Mater.* **2**, 1056–1085 (2012).
101. Phan, V. P., Pecquenard, B. & Le Cras, F. High-performance all-solid-state cells fabricated with silicon electrodes. *Adv. Funct. Mater.* **22**, 2580–2584 (2012).
102. Kanazawa, S., Baba, T., Yoneda, K., Mizuhata, M. & Kanno, I. Deposition and performance of all solid-state thin-film lithium-ion batteries composed of amorphous Si/LiPON/VO-LiPO multilayers. *Thin Solid Films* **697**, 137840 (2020).
103. Tron, A., Nosenko, A., Park, Y. D. & Mun, J. Enhanced ionic conductivity of the solid electrolyte for lithium-ion batteries. *J. Solid State Chem.* **258**, 467–470 (2018).
104. Feng, Q., Xie, X., Zhang, M. & Liao, N. Superior interfacial stability and conductivity of B-doped LiPON electrolyte for LiCoO2 electrode in solid-state lithium batteries. *Colloids Surf. A Physicochem. Eng. Asp* **648**, 129349 (2022).
105. Song, X. et al. Enhancement of Mn-doped LiPON electrolyte for higher performance of all-solid-state thin film lithium battery. *Mater. Today Phys.* **33**, 101037 (2023).
106. Doux, J. M. et al. Pressure effects on sulfide electrolytes for all solid-state batteries. *J. Mater. Chem. A* **8**, 5049–5055 (2020).
107. Zou, C. et al. LiAlO2-coated LiNi0.8Co0.1Mn0.1O2 and chlorine-rich argyrodite enabling high-performance all-solid-state lithium batteries at suitable stack pressure. *Ceram. Int.* **49**, 443–449 (2023).
108. Chen, M. et al. Achieving micron-scale plasticity and theoretical strength in Silicon. *Nat. Commun.* **11**, 1–10 (2020).
109. Zhu, Y., Xu, F., Qin, G., Fung, W. Y. & Lu, W. Mechanical properties of vapor - Liquid - Solid synthesized silicon nanowires. *Nano Lett.* **9**, 3934–3939 (2009).
110. Horowitz, Y., Strauss, E., Peled, E. & Golodnitsky, D. How to Pack a Punch – Why 3D Batteries are Essential. *Israel J. Chem.* **61**, 38–50 (2021).
111. Li, Y. et al. Advanced architecture designs towards high-performance 3D microbatteries. *Nano Mater. Sci.* **3**, 140–153 (2021).
112. Yue, C., Li, J. & Lin, L. Fabrication of Si-based three-dimensional microbatteries: a review. *Front. Mech. Eng.* **12**, 459–476 (2017).
113. Moitzheim, S. et al. Toward 3D thin-film batteries: optimal current-collector design and scalable fabrication of TiO2 thin-film electrodes. *ACS Appl. Energy Mater.* **2**, 1774–1783 (2019).
114. Baggetto, L., Niessen, R. A. H., Roozehoom, F. & Notten, P. H. L. High energy density all-solid-state batteries: a challenging concept towards 3D integration. *Adv. Funct. Mater.* **18**, 1057–1066 (2008).
115. Mubarak, S., Dhamodharan, D. & Byun, H. S. Recent advances in 3D printed electrode materials for electrochemical energy storage devices. *J. Energy Chem.* **81**, 272–312 (2023).
116. Lyu, Z. et al. Design and manufacture of 3D-Printed. *Batteries. Joule* **5**, 89–114 (2021).
117. Beydaghi, H. et al. 3D printed silicon-few layer graphene anode for advanced Li-ion batteries. *RSC Adv.* **11**, 35051–35060 (2021).
118. Drews, M. et al. Towards 3D-lithium ion microbatteries based on silicon/graphite blend anodes using a dispenser printing technique. *RSC Adv.* **10**, 22440–22448 (2020).
119. Yue, C. et al. Fabrication of Multilayer Si/TiN/Sb NR Arrays as Anode for 3D Si-Based Lithium/Sodium Ion Microbatteries. *Adv. Mater. Interfaces* **7**, 1–10 (2020).
120. Refino, A. D. et al. Versatilely tuned vertical silicon nanowire arrays by cryogenic reactive ion etching as a lithium-ion battery anode. *Sci. Rep.* **11**, 1–15 (2021).
121. Nugroho, A. P. et al. Vertically aligned n-type silicon nanowire array as a free-standing anode for lithium-ion batteries. *Nanomaterials* **11**, 3137 (2021).
122. Singh, N., Sahoo, M. K. & Kale, P. G. Effect of MACE parameters on length of porous silicon nanowires (PSiNWs). *J. Cryst. Growth* **496–497**, 10–14 (2018).
123. Leonardi, A. A., Faro, M. J., Lo & Irrera, A. Silicon nanowires synthesis by metal-assisted chemical etching: a review. *Nanomaterials* **11**, 1–24 (2021).
124. Plugaru, R. et al. Structure and electrical behavior of silicon nanowires prepared by MACE process. *Surf. Interfaces* **33**, 102167 (2022).
125. Refino, A. D. et al. Impact of exposing lithium metal to monocrystalline vertical silicon nanowires for lithium-ion microbatteries. *Commun. Mater.* **4**, 1–11 (2023).
126. Eldona, C. et al. A Free-Standing Polyaniline/Silicon Nanowire Forest as the Anode for Lithium-ion Batteries. *Chem. – An Asian J.* e202200946 (2022).
127. Kang, J. et al. How electrode thicknesses influence performance of cylindrical lithium-ion batteries. *J. Energy Storage* **46**, 103827 (2022).
128. Doyle, M., Fuller, T. F. & Newman, J. Modeling of Galvanostatic Charge and Discharge of the Lithium/Polymer/Insertion Cell. *J. Electrochem. Soc.* **140**, 1526–1533 (1993).
129. Du, Z., Wood, D. L., Daniel, C., Kalnaus, S. & Li, J. Understanding limiting factors in thick electrode performance as applied to high energy density Li-ion batteries. *J. Appl. Electrochem.* **47**, 405–415 (2017).
130. Chen, D., Lou, Z., Jiang, K. & Shen, G. Device configurations and future prospects of flexible/stretchable lithium-ion batteries. *Adv. Funct. Mater*. **28**, 1805596 (2018).
131. Ni, J., Dai, A., Yuan, Y., Li, L. & Lu, J. Three-dimensional microbatteries beyond lithium ion. *Matter* **2**, 1366–1376 (2020).
132. Xu, J. et al. Three-dimensional structural engineering for energy-storage devices: from microscope to macroscope. *ChemElectroChem* **1**, 975–1002 (2014).
133. Zhu, Z. et al. Recent advances in high-performance microbatteries: construction, application, and perspective. *Small* **16**, 1–28 (2020).
134. Xu, K. et al. Design and 3D printing of interdigitated electrode structures for high-performance full lithium-ion battery. *Chin. J. Mech. Eng. Addit. Manuf. Front.* **1**, 100053 (2022).
135. Frith, J. T., Lacey, M. J. & Ulissi, U. A non-academic perspective on the future of lithium-based batteries. *Nat. Commun.* **14**, 1–17 (2023).
136. Pikul, J. H., Gang Zhang, H., Cho, J., Braun, P. V. & King, W. P. High-power lithium ion microbatteries from interdigitated three-dimensional bicontinuous nanoporous electrodes. *Nat. Commun.* **4**, 1–5 (2013).

137. Hamdana, G. et al. Towards fabrication of 3D isotopically modulated vertical silicon nanowires in selective areas by nanosphere lithography. *Microelectron. Eng.* **179**, 74–82 (2017).
138. Wasisto, H. S. et al. Femtogram aerosol nanoparticle mass sensing utilising vertical silicon nanowire resonators. *Micro. Nano Lett.* **8**, 554–558 (2013).
139. Hamdana, G. et al. Nanoindentation of crystalline silicon pillars fabricated by soft UV nanoimprint lithography and cryogenic deep reactive ion etching.*Sens. Actuators A Phys.* **283**, 65–78 (2018).
140. Merzsch, S. et al. Production of vertical nanowire resonators by cryogenic-ICP-DRIE. *Microsyst. Technol.* **20**, 759–767 (2014).
141. Wasisto, H. S. et al. Silicon resonant nanopillar sensors for airborne titanium dioxide engineered nanoparticle mass detection. *Sens. Actuators B Chem.* **189**, 146–156 (2013).
142. Lethien, C. et al. Micro-patterning of LiPON and lithium iron phosphate material deposited onto silicon nanopillars array for lithium ion solid state 3D micro-battery. *Microelectron. Eng.* **88**, 3172–3177 (2011).
143. Sternad, M., Forster, M. & Wilkening, M. The microstructure matters: breaking down the barriers with single crystalline silicon as negative electrode in Li-ion batteries. *Sci. Rep.* **6**, 2–9 (2016).
144. Gerasopoulos, K. et al. Hierarchical three-dimensional microbattery electrodes combining bottom-up self-assembly and top-down micromachining. *ACS Nano* **6**, 6422–6432 (2012).
145. Poodt, P. et al. Spatial atomic layer deposition: a route towards further industrialization of atomic layer deposition. *J. Vac. Sci. Technol. A Vacuum Surf. Film.* **30**, 010802 (2012).
146. Yadav, A., De, B., Singh, S. K., Sinha, P. & Kar, K. K. Facile development strategy of a single carbon-fiber-based all-solid-state flexible lithium-ion battery for wearable electronics. *ACS Appl. Mater. Interfaces* **11**, 7974–7980 (2019).
147. Talin, A. A. et al. Fabrication, testing, and simulation of all-solid-state three-dimensional li-ion batteries. *ACS Appl. Mater. Interfaces* **8**, 32385–32391 (2016).
148. Li, Y. et al. Microbatteries with twin-Swiss-rolls redefine performance limits in the sub-square millimeter range. *Nanoscale Horizons* **8**, 127–132 (2023).
149. Si, W. et al. A single rolled-Up Si tube battery for the study of electrochemical kinetics, electrical conductivity, and structural integrity. *Adv. Mater.* **26**, 7973–7978 (2014).
150. Bermejo, D. & Cardona, M. Raman scattering in pure and hydrogenated amorphous. *J. Non. Cryst. Solids* **32**, 405–419 (1978).
151. Liu, Y., Zhu, Y. & Cui, Y. Challenges and opportunities towards fast-charging battery materials. *Nat. Energy* **4**, 540–550 (2019).
152. Liu, L. et al. Artificial electrode interfaces enable stable operation of freestanding anodes for high-performance flexible lithium ion batteries. *J. Mater. Chem. A* **7**, 14097–14107 (2019).
153. Luais, E. et al. Mesoporous silicon negative electrode for thin film lithium-ion microbatteries. *J. Power Sour.* **274**, 693–700 (2015).
154. Chen, X. et al. High rate performance of virus enabled 3D n-type Si anodes for lithium-ion batteries. *Electrochim. Acta* **56**, 5210–5213 (2011).
155. Yue, C. et al. Laser-patterned Si/TiN/Ge anode for stable Si based Li-ion microbatteries. *J. Power Sour.* **493**, 229697 (2021).
156. Guo, K. et al. Hierarchical microcables constructed by CoP@C⊂Carbon framework intertwined with carbon nanotubes for efficient lithium storage. *Adv. Energy Mater.* **10**, 1–9 (2020).
157. Krauskopf, T., Richter, F. H., Zeier, W. G. & Janek, J. Physicochemical concepts of the lithium metal anode in solid-state batteries. *Chem. Rev.* **120**, 7745–7794 (2020).
158. Liu, Q. Q., Xiong, D. J., Petibon, R., Du, C. Y. & Dahn, J. R. Gas evolution during unwanted lithium plating in Li-Ion cells with EC-based or EC-Free Electrolytes. *J. Electrochem. Soc.* **163**, A3010–A3015 (2016).
159. Petibon, R., Harlow, J., Le, D. B. & Dahn, J. R. The use of ethyl acetate and methyl propanoate in combination with vinylene carbonate as ethylene carbonate-free solvent blends for electrolytes in Li-ion batteries. *Electrochim. Acta* **154**, 227–234 (2015).
160. Fan, T. et al. Operating highly stable LiCoO2 cathodes up to 4.6 V by using an effective integration of surface engineering and electrolyte solutions selection. *Adv. Funct. Mater.* **32**, 2204972 (2022).
161. Ferrari, S. et al. Latest advances in the manufacturing of 3D rechargeable lithium microbatteries. *J. Power Sour.* **286**, 25–46 (2015).
162. Liu, X. H. et al. Size-dependent fracture of silicon nanoparticles during lithiation. *ACS Nano* **6**, 1522–1531 (2012).
163. Lee, S. W., McDowell, M. T., Berla, L. A., Nix, W. D. & Cui, Y. Fracture of crystalline silicon nanopillars during electrochemical lithium insertion. *Proc. Natl. Acad. Sci. USA.* **109**, 4080–4085 (2012).
164. Vorobyev, A. Y. & Guo, C. Direct femtosecond laser surface nano/microstructuring and its applications. *Laser. Photonics Rev.* **7**, 385–407 (2013).
165. Wang, Q. & Zhou, W. Direct fabrication of cone array microstructure on monocrystalline silicon surface by femtosecond laser texturing. *Opt. Mater.* **72**, 508–512 (2017).
166. Ahn, S., Hwang, D. J., Park, H. K. & Grigoropoulos, C. P. Femtosecond laser drilling of crystalline and multicrystalline silicon for advanced solar cell fabrication. *Appl. Phys. A Mater. Sci. Process.* **108**, 113–120 (2012).
167. Chu, D., Yao, P. & Huang, C. Anti-reflection silicon with self-cleaning processed by femtosecond laser. *Opt. Laser Technol.* **136**, 106790 (2021).
168. Moram, S. S. B., Byram, C. & Soma, V. R. Femtosecond laser patterned silicon embedded with gold nanostars as a hybrid SERS substrate for pesticide detection. *RSC Adv.* **13**, 2620–2630 (2023).
169. Selinis, P. & Farmakis, F. Review—A Review on the anode and cathode materials for lithium-ion batteries with improved Subzero temperature performance. *J. Electrochem. Soc.* **169**, 010526 (2022).
170. Ordoñez, J., Gago, E. J. & Girard, A. Processes and technologies for the recycling and recovery of spent lithium-ion batteries. *Renew. Sustain. Energy Rev.* **60**, 195–205 (2016).
171. Mawani, H. D., Shastri, N. M., Mangrola, M. H. & Joshi, V. G. Structural and electrical properties of sodium bismuth titanate prepared by solid state reaction method. In *AIP Conference Proceedings* 2220 5991–6002 (Springer Science and Business Media Deutschland GmbH, 2020).
172. Wang, Y. & Huang, H. Y. S. An overview of lithium-ion battery cathode materials. In *Materials Research Society Symposium Proceedings* 1363 43–48 (Springer, 2011).
173. Ruzmetov, D. et al. Electrolyte stability determines scaling limits for solid-state 3D Li ion batteries. *Nano Lett* **12**, 505–511 (2012).
174. Ko, W. Y., Fang, M. J., Li, M. S. & Lin, K. J. Fabrication of self-standing Si-TiO2 web-nanowired anodes for high volumetric capacity lithium ion microbatteries. *Nano Express* **1**, 030014 (2020).

Acknowledgements

This work was conducted within a project of SiNanoBatt funded by the German Federal Ministry of Education and Research (BMBF) and Indonesia Endowment Fund for Education (LPDP) under the Southeast Asia – Europe Joint Funding Scheme for Research and Innovation. Andam Deatama Refino acknowledges the Ministry of Research, Technology and Higher Education of the Republic of Indonesia (RISTEKDIKTI) for the Ph.D. scholarships of BPP-LN under no. T/912/D3.2/KD.02.01/2019. Support from the Indonesian-German Centre for Nano and Quantum Technologies (IG-Nano) is also acknowledged. The project (19ENG05 NanoWires) has received funding from the EMPIR program co-financed by the Participating States and from the European Union's Horizon 2020 research and innovation program.

Author contributions

H.S.W. and A.D.R. conceived the idea and concept, wrote the initial manuscript, validated the discussion, and revised the paper. A.D.R., C.E., R.F.H.H. and E.A. contributed to the writing of different sections. H.S.W., E.P. and A.S. supervised the work, led the project, contributed to the final writing, and acquired the funding. All authors discussed and approved the final manuscript.

Funding

Open Access funding enabled and organized by Projekt DEAL.

Competing interests

The authors declare no competing interests.

Additional information

Supplementary information The online version contains supplementary material available at https://doi.org/10.1038/s43246-024-00459-7.

Correspondence and requests for materials should be addressed to Andam Deatama Refino or Hutomo Suryo Wasisto.

Peer review information *Communications Materials* thanks Michael Sternad, Christopher Choi and the other, anonymous, reviewer(s) for their contribution to the peer review of this work. Primary Handling Editors: Jet-Sing Lee. A peer review file is available.